



Entergy Operations, Inc.
1340 Echelon Parkway
Jackson, Mississippi 39213-8298
Tel 601-368-5758

F. G. Burford
Acting Director
Nuclear Safety & Licensing

CNRO-2004-00026

May 4, 2004

U. S. Nuclear Regulatory Commission
Attn.: Document Control Desk
Washington, DC 20555-0001

SUBJECT: Request for Alternative ANO1-R&R-006 -
Proposed Alternative to ASME Weld Examination Requirements for
Repairs Performed on Reactor Vessel Head Penetration Nozzles

Arkansas Nuclear One, Unit 1
Docket No. 50-313
License No. DPR-51

- REFERENCES:**
1. Entergy Operations, Inc. letter CNRO-2004-00022 to the NRC dated April 8, 2004
 2. Entergy Operations, Inc. letter CNRO-2002-00054 to the NRC dated November 26, 2002
 3. Entergy Operations, Inc. letter CNRO-2004-00014 to the NRC dated March 4, 2004
 4. NRC letter to Entergy Operations, Inc. (TAC No. MB6599) dated November 6, 2003

Dear Sir or Madam:

In Reference 1, Entergy Operations, Inc., (Entergy) submitted revised Request for Alternative ANO1-R&R-006 for use at Arkansas Nuclear One, Unit 1 (ANO-1). Specifically, this request proposes an alternative to the requirements to evaluate actual flaw characteristics as defined in ASME Section III NB-5330(b) and ASME Section XI IWA-3300, IWB-3142.4, IWB-3420, and IWB-3613(b).

On April 30, 2004, the NRC staff provided a Request for Additional Information (RAI) to Entergy pertaining to ANO1-R&R-006. Representatives from the NRC staff and Entergy discussed this RAI in a telephone call. Entergy's response to the RAI is provided in Enclosure 1. As a result of the RAI, Entergy supercedes ANO1-R&R-006 as submitted via Reference 1 with a revised request contained in Enclosure 2.

A047

Provided in Enclosure 3 is the technical report that supports revised request ANO1-R&R-006. This report satisfies a commitment made to the NRC in Reference 1 in which Entergy committed to submit its final technical basis, including the flaw evaluation, by June 1, 2004.

In addition, Entergy previously submitted to the NRC the following documents that supported the previous version of ANO1-R&R-006:

- ANO Calculation 86-E-0074-160 (Reference 2)
- ANO Calculation 86-E-0074-161 (Reference 2)
- ANO Calculation 86-E-0074-164 (Reference 2)
- Engineering Report M-EP-2004-002 (Reference 3)

These documents remain applicable to the enclosed revised version of ANO1-R&R-006.

This letter contains no commitments.

Should you have any questions regarding this letter, please contact Guy Davant at (601) 368-5756.

Very truly yours,



FGB/GHD/ghd

Enclosures: 1. Response to NRC Request for Additional Information (Revised 4/30/04)
2. Request for Alternative ANO1-R&R-006
3. Technical Report Supporting ANO1-R&R-006

cc: Mr. W. A. Eaton (ECH)
Mr. J. S. Forbes (ANO)

Dr. Bruce. S. Mallett
Regional Administrator, Region IV
U. S. Nuclear Regulatory Commission
611 Ryan Plaza Drive, Suite 400
Arlington, TX 76011-8064

U. S. Nuclear Regulatory Commission
Attn: Mr. T. W. Alexion
MS O-7 D1
Washington, DC 20555-0001

NRC Senior Resident Inspector
Arkansas Nuclear One
P. O. Box 310
London, AR 72847

ENCLOSURE 1

CNRO-2004-00026

**RESPONSE TO NRC REQUEST FOR ADDITIONAL INFORMATION
(REVISED 4/30/04)**

REQUEST FOR ADDITIONAL INFORMATION (REVISED 04/30/04)
RELIEF REQUEST ANO1-R&R-006
ARKANSAS NUCLEAR ONE, UNIT 1 (ANO-1)

1. Describe briefly the latest technical basis in support of Relief Request R&R-006, including the following items:

- 1a. Methodology - Discuss the steps of elastic plastic fracture mechanics (EPFM) approach; discuss the applicability of the EPFM for the ferritic reactor vessel head material in the flaw evaluation; and provide references.

Response:

The method for the EPFM analysis and its applicability are discussed on pages 35 and 36 of the technical report (Enclosure 3). References are noted in the description. Details of the method are presented on pages 35 through 43 of the report.

- 1b. Assumptions - Discuss flaw size, flaw path; the applicability of the upper shelf energy value used for the ANO-1 reactor vessel head; and provide references.

Response:

1) *Flaw size and flaw path are the same as that used for the LEFM analysis and are presented on pages 11, 12, 42, and 43 of the technical report (Enclosure 3).*

2) *The applicability of the upper shelf energy value is discussed in pages 36 through 38 of the technical report (Enclosure 3). The references are cited in the discussion and are provided at the end of the report.*

- 1c. Results - Discuss the preliminary results in terms of safety factors, J applied, and J material values; and flaw growth.

Response:

The results of the analysis with respect to the use of safety factors, applied J, and J material toughness are presented on pages 43 through 46 of the technical report (Enclosure 3). The fatigue crack growth is discussed on pages 33 and 34 of the report.

- 1d. Preliminary Conclusion - Entergy needs to make a preliminary conclusion regarding whether the postulated flaw in the J-groove weld remnant will affect the structural integrity of the ANO-1 reactor vessel head.

Response:

- 1) *The discussion of the analysis results and that of the ASME Code review and its applicability for the postulated J-groove weld remnant are presented on pages 48 through 52 of the technical report (Enclosure 3).*
 - 2) *The conclusion, based on the analytical effort, is presented on pages 53 and 54 of the technical report (Enclosure 3).*
2. Entergy needs to make a preliminary conclusion regarding whether the nozzle repair proposed in Request ANO1-R&R-006 will affect the reactor vessel head in maintaining the structural integrity and leakage integrity of the reactor coolant system.

Response:

The evaluation of the new repair weld impact on the remnant J-groove weld is presented on pages 46 and 47 of the technical report (Enclosure 3). Conclusions are provided on pages 53 and 54 of the report.

3. Entergy needs to commit to submit its final technical basis, including the flaw evaluation, by a certain date. Entergy had proposed June 1, 2004, in its April 12, 2004 submittal.

Response:

The final technical basis supporting ANO1-R&R-006 is documented in the technical report (Enclosure 3). Therefore, this commitment is met.

ENCLOSURE 2

CNRO-2004-00026

**REQUEST FOR ALTERNATIVE
ANO1-R&R-006, Rev. 0**

**ENTERGY OPERATIONS, INC.
ARKANSAS NUCLEAR ONE, UNIT 1
3rd 10-YEAR INTERVAL
REQUEST No. ANO1-R&R-006, Rev. 0**

REFERENCE CODE:

The original code of construction for Arkansas Nuclear One, Unit 1 (ANO-1) is ASME Section III, 1965 Edition with Addenda through Summer, 1967. The components (including supports) may meet the requirements set forth in subsequent editions and addenda of the ASME Code incorporated by reference in 10 CFR 50.55a(b) subject to the limitations and modifications listed therein and subject to NRC approval. The codes of record for the repairs described within this request are the 1989 Edition of ASME Section III and 1992 Edition of ASME Section XI codes. ANO-1 is in its third (3rd) 10-Year Inservice Inspection interval.

I. System/Component(s)

a) Name of Component:

Reactor Pressure Vessel (RPV) head nozzles (There are 69 nozzles welded to the RPV head. This request applies to all 69 RPV head penetration nozzles, including the 6 that were repaired using the approved alternative ANO1-R&R-004 during the previous refueling outage.¹)

b) Function:

- The J-groove weld remnant left in place serves no function. It becomes nothing more than a remaining weldment attached to the RPV head.
- Any new repair welds serve as the pressure boundary weld for the RPV head nozzle and RPV head.

c) ASME Code Class:

The RPV head and RPV head nozzles are ASME Class 1.

d) Category:

Examination Category B-E, Pressure Retaining Partial Penetration Welds in Vessels; Item No. B4.12

II. Code Requirements

A. ASME Section XI (pertaining to the J-groove weld remnant)

Paragraph IWA-4310 requires in part that "Defects shall be removed or reduced in size in accordance with this Paragraph." Furthermore, IWA-4310 allows that "...the defect removal and any remaining portion of the flaw may be evaluated and the component accepted in

¹ Request for Alternative ANO1-R&R-004 (TAC No. MB6599) was approved by the NRC in a letter dated November 25, 2003.

accordance with the appropriate flaw evaluation rules of Section XI.” The ASME Section XI, IWA-3300 rules require characterization of flaws detected by inservice examination.

Paragraph IWB-3420 requires the characterization of flaws in accordance with the rules of IWA-3300.

Subparagraph IWB-3142.4 allows the use of analytical evaluation to demonstrate that a component is acceptable for continued service. It also requires that components found acceptable for continued service by analytical evaluation be subject to successive examination during the next three inspection periods.

Paragraph IWB-3613 establishes acceptance criteria to be used for evaluating flaws in areas where bolt-up loads play a significant role (i.e., the RPV-to-head interface). IWB-3613(b) requires the use of a safety factor of $\sqrt{10}$ (3.16) to determine the stress intensity factor (SIF) of a flaw during normal operating conditions.

B. ASME Section III (pertaining to the new repair weld)

Section III Subsection NB-5330(b) states, “Indications characterized as cracks, lack of fusion, or incomplete penetrations are unacceptable regardless of length.”

III. Proposed Alternative

Pursuant to 10 CFR 50.55a(a)(3)(i), Entergy proposes the following alternative to ASME Section XI IWB-3420/IWA-3300, IWB-3142.4, IWB-3613(b), and Section III NB-5330(b) as they pertain to the examination and evaluation of the repair weld and the remnant J-groove weld of the RPV head penetration nozzle that is not removed. Specifically, this alternative involves:

- Leaving a remnant of the J-groove weld in place following repair activities and operating with safety factors of 3 (primary stresses) and 1.5 [secondary stresses (which include residual stresses)] on fracture mechanics parameters until the ANO-1 RPV head is replaced during the next refueling outage (1R19)
- Examining the repair weld

Each aspect is discussed below.

A. The Remnant J-Groove Weld

The planned repair for the subject RPV head nozzles does not include removing any cracks discovered in the remaining J-groove partial penetration welds. Therefore, per the requirements of IWA-4310, the cracks must be evaluated using the appropriate flaw evaluation rules of Section XI. No additional inspections can be performed to characterize the cracks due to the configuration of the nozzle and the weld. Thus, the actual dimensions of the crack cannot be fully determined as required by IWA-3300.

In lieu of fully characterizing any existing cracks, Entergy used worst-case assumptions to conservatively estimate the crack extent and orientation. The postulated crack extent and orientation were evaluated using linear elastic fracture mechanics (LEFM) and elastic plastic fracture mechanics (EPFM) methods. This evaluation, in conjunction with this request,

justifies leaving the remnant weld in place without performing successive examinations in accordance with IWB-3142.4.

The evaluation also determined that the results of the fracture mechanics analysis meet safety factors of 3 and 1.5 for primary and secondary stresses, respectively.

B. Examining the Repair Weld

The new pressure boundary repair weld that connects the remaining portion of the RPV head nozzles to the low alloy RPV head contains a material "triple point." The triple point is located at the root of the weld where the Alloy 600 nozzle will be welded with Alloy 690 (52) filler material to the SA-533 Grade B, Class 1 Mn-Mo low alloy steel plate (See Figures 2 and 3). Experience has shown that during solidification of the Alloy 52 weld filler material, a lack of fusion (otherwise known as a welding solidification anomaly) area may occur at the root of the partial penetration welds.

Entergy is requesting relief from the requirement of NB-5330(b) regarding the potential lack of fusion at the root of the repair weld. If a weld triple point anomaly occurs in any of the repair welds, it will be evaluated in accordance with the appropriate flaw evaluation rules of ASME Section XI. Calculations have been completed to justify this welding solidification anomaly.²

IV. Basis and Justification for Proposed Alternative

Inspections of the RPV head will be performed in accordance with revised NRC Order EA-03-009, *Issuance of Order Establishing Interim Inspection Requirements for Reactor Pressure Vessel Heads at Pressurized Water Reactors*, dated February 20, 2004 and/or approved relaxation requests. These inspections may identify conditions that indicate a need to repair flaws discovered in the RPV head penetrations. The use of any of the alternatives permitted by the applicable ASME Codes for repairs will result in increased radiation dose with no compensating increase in quality or safety. The post-weld heat treatment (PWHT) parameters required by NB-4622 would be difficult to achieve on a RPV head in containment and would pose significant risk of distortion to the geometry of the RPV head and vessel head penetrations. In addition, the existing J-groove welds would be exposed to PWHT for which they were not qualified. This request applies to repair of any or all of the 69 RPV head penetrations.

A. The Remnant J-Groove Weld

The requirements of IWA-4310 allow two options for determining the disposition of discovered cracks. The subject cracks are either removed as part of the repair process or left as-is and evaluated per the rules of IWB-3600. The repair design specifies the inside corner of the J-groove weld be progressively chamfered from the center to outermost penetrations to maintain an acceptable flaw size. Section III paragraph NB-3352.4(d)(3) requires that the corners of the end of each nozzle to be rounded to a radius of $\frac{1}{2} t_n$ or $\frac{3}{4}$ inch whichever is smaller. A 1/8-inch minimum chamfer considered equivalent to the radius specified in NB-3352.4(d)(3) will be incorporated on the bottom corner of the repaired RPV head nozzle penetrations in lieu of the radius. The radius is specified to reduce the stress concentration that might occur at a sharp corner; however, since the original partial penetration weld that remains in this area is analyzed assuming through-weld cracks exist therein the presence or

² See ANO Calculation E-86-0074-161 submitted to the NRC via Entergy letter CNO-2002-00054 dated November 26, 2002.

absence of a radius or chamfer at this location is not significant with respect to stress concentration. The primary purpose of the chamfer is to assure that any remaining cracks are no larger than those assumed for the analysis.

The assumptions of IWB-3600 are that the cracks are fully characterized to be able to compare the calculated crack parameters to the acceptable parameters addressed in IWB-3500. In the alternative being proposed, the acceptance of the postulated crack is calculated based on the two inputs of expected crack orientation and the geometry of the weld. Typically, an expected crack orientation is evaluated based on prevalent stresses at the location of interest. In these welds, operating and residual stresses are obtained using finite element analysis of the RPV head. Since hoop stresses will be the dominant stress as determined by calculations, it is expected that radial type cracks (with respect to the penetration) will occur. Using worst case (maximum) assumptions with the geometry of the as-left weld, the postulated crack will be assumed to begin at the intersection of the RPV head inner diameter surface and the RPV head nozzle bore and propagate to the RPV head-to-butter interface. The depth and orientation are worst-case assumptions for cracks that may occur in the remaining J-groove partial penetration weld configuration.

The original nozzle-to-RPV head weld configuration is extremely difficult to UT due to the compound curvature and fillet radius as can be seen in Figures 2 and 3. These conditions preclude ultrasonic coupling and control of the sound beam in order to perform flaw sizing with reasonable confidence in the measured flaw dimension. Therefore it is impractical, and presently, the technology does not exist, to characterize flaw geometries that may exist therein. Not only is the configuration not conducive to UT but the dissimilar metal interface between the Ni-Cr-Fe weld and the low alloy steel RPV head increases the UT difficulty. Furthermore, due to limited accessibility from the RPV head outer surface and the proximity of adjacent nozzle penetrations, it is impractical to scan from this surface on the RPV head base material to detect flaws in the vicinity of the original weld. Entergy proposes to accept these flaws by analysis of the worst case that might exist in the J-groove. Since the worst case condition is to be analyzed as described below, no future examinations of these flaws is planned.

As previously discussed, after boring and removing the nozzle end, the remaining J-groove weld material will be chamfered to reduce the SIF.

Since the hoop stresses in the J-groove weld are generally about two times the axial stress at the same location, the preferential direction for cracking is axial, or radial relative to the nozzle. A radial crack in the Alloy 182 weld metal is postulated to propagate by primary water stress corrosion cracking (PWSCC) through the weld and butter, to the interface with the low alloy steel RPV head.

Detailed analyses, including residual stress evaluation and fracture mechanics, have been performed to establish the chamfer design that will result in an applied SIF at the interface between Inconel alloy 600 butter weld and the low alloy steel reactor vessel head. This SIF exceeds the ASME Section XI allowable limit for normal-upset conditions using a safety factor of $\sqrt{10}$ per IWB-3613(b). The analyses were performed for an outermost nozzle penetration location (38.5°), which provides a bounding analysis for the other nozzles in the RPV head.

The residual stress analyses were performed using finite element methods that have been developed by Dominion Engineering Inc. for evaluating RPV head penetration J-groove weld residual stresses. The analyses are similar to those that supported various relaxation

requests to NRC Order EA-03-009 that have been approved by the NRC staff.³ The analyses simulate the original installation of the RPV head penetration nozzle. The process includes the installation of the butter layer followed by a post-weld heat treatment, J-groove welding of the nozzle followed by a Code hydro-test and subsequent steady state operation. Upon achieving ambient conditions the nozzle was removed. At this point, variations in chamfering depths were modeled, each model subjected to a normal heat-up followed by a steady state condition and then a cooldown to ambient. Two additional transient conditions, starting from an initial steady state condition, representing a reactor trip (normal and upset condition) and rod withdrawal (accident condition) were analyzed. This completes the full spectrum of the required analysis for performing finite element based fracture mechanics evaluations.

The fracture mechanics analysis uses a finite element model similar to that used in the residual stress analysis. The finite element model has a refined mesh that includes crack tip elements along the interface between the Inconel Alloy 600 butter weld and the low alloy carbon steel RPV head. This model simulates a fully cracked J-groove weld including the butter layer. The fracture mechanics analysis was performed using a linear elastic superposition method. Relaxing the residual stresses due to cracking was not utilized since the analysis used a linear elastic formulation. The SIFs were obtained at several locations along the postulated crack front. The stresses obtained from the residual and operating stress analysis were entered as crack face pressure. Reactor vessel internal pressure on the crack face was added to the distribution obtained from the stress analysis.

The stress plots at selected locations in the finite element stress analysis for non-steady state operation (i.e., heat-up, cool-down, reactor trip, and rod withdrawal) were reviewed to capture the maximum stress during the specific condition. In this manner, the SIF was maximized for use in fatigue evaluations.

The fracture mechanics analysis produced SIFs along the crack front for the conditions evaluated. The conditions evaluated were:

- 1) Normal steady state operation;
- 2) Normal heat-up from ambient condition;
- 3) Normal cool-down from steady state condition;
- 4) Reactor trip from steady state condition; and,
- 5) Rod withdrawal accident from steady state condition.

The obtained SIFs were compared to the applicable ASME Code Section XI IWB-3613(b) value for the specified condition of operation.

³ See letters to Entergy from the NRC dated October 9, 2003, November 7, 2003, and November 12, 2003.

The NRC has documented its position for fracture mechanics analysis as follows:

So far, the NRC accepted only an approach of applying residual stresses directly on crack faces (i.e., as primary stresses) for various applications related to reactor pressure vessels, control rod drive mechanism (CRDM) penetrations, and in-core instrument (ICI) nozzles.⁴

A summary of the results from LEFM analysis, which was performed in accordance with this guidance for the various assumed J-groove weld configurations, is presented in Table 1. In this analysis, the LEFM analysis was performed to evaluate the remnant J-groove weld by applying the stresses due to operating pressure, temperature gradients, and residual stress effects on the crack face as primary stresses. Table 1 below shows that 13 of 16 values for maximum SIF obtained from these analyses exceed the currently allowable fracture toughness of 63.2 ksi√in in accordance with the $\sqrt{10}$ criterion of ASME Section XI, IWB-3613(b).

Table 1: Maximum SIF from Fracture Mechanics Analysis

J-groove Weld Remnant Configuration	Maximum Applied Stress Intensity Factor ¹ (ksi√in)		
	Steady State Operation ²	Residual Stresses Only ³	Operating Condition Only ⁴
No Chamfer	77.4 – Downhill 103.4 - Uphill	75.3 – Downhill 115.7 – Uphill	2.1 - Downhill Note 5 – Uphill
Design Minimum Chamfer	80.0 –Downhill 94.4 - Uphill	76.99 – Downhill 90.7 – Uphill	3.01 – Downhill 3.7 – Uphill
Design Maximum Chamfer	79.4 – Downhill 84.8 - Uphill	76.38 – Downhill 81.1 – Uphill	3.02 – Downhill 3.7 - Uphill
Theoretical Maximum Chamfer	65.2 – Downhill 62.5 - Uphill	62.19 – Downhill 58.85 – Uphill	3.01 – Downhill 3.65 - Uphill

Notes:

- 1) The applied SIF is based on considering the three conditions discussed in 2, 3, and 4, below.
- 2) The steady state condition is the combined SIF based on residual stress plus the steady state operating stresses (pressure and temperature).
- 3) The residual stress condition is based on the residual stress state after completion of the specific operation on the J-groove weld as indicated by the configuration column.
- 4) The operating condition is the difference between the steady state condition and the residual stress state. This column provides the SIF estimate due to the operating condition alone.
- 5) The SIF due to the residual stress is higher than at steady state operating condition.

⁴ See NRC letter, *Request for Additional Information Concerning WCAP-16180NP, Revision 0, "Operability Assessment for Combustion engineering Plants with Hypothetical Flaw Indications in Pressurizer heater Sleeves"* (TAC No. MC1751) from Mr. D. Holland, Project Manager, Office of NRR, to Mr. G. Bischoff, Manager, Owners Group Program Management Office, Westinghouse Electric Company.

The expected fatigue crack growth for a period including two operating cycles were analyzed using the expected transient operating conditions. These analyses, as presented in the supporting technical report (Enclosure 3 of letter CNRO-2004-00026), show that the extension of the postulated crack due to the anticipated fatigue cycles to be 0.005 inch. This expected crack growth is insignificant compared to the initial postulated crack size (1.5 inches) and, hence, would not contribute significantly to the SIF results presented above.

Since the LEFM analysis presented above shows that the acceptance criterion [specified in ASME Section XI IWB-3613(b)] was not satisfied, EPFM analysis was also performed. The EPFM methodology followed the guidance presented in Appendix K of ASME Section XI. However, the equations for SIF determination in Appendix K were not used since they do not apply to the geometry of the crack evaluated. Instead, the SIF values used in the analysis were obtained from the LEFM analysis presented above.

For the EPFM analysis, the material toughness determination was made using accepted methods as described in detail in the enclosed technical report. The method used to estimate the material fracture toughness behavior followed the guidance provided by the NRC.⁵ The Charpy upper shelf energy (USE) for the ANO-1 RPV head was estimated using an accepted method as delineated in the enclosed technical report. The method to estimate the applied J-integral from LEFM determined SIF (K) followed the guidance in Appendix K of ASME Section XI. This is an acceptable method based on general fracture mechanics principles.⁶ The applicability of the EPFM method was demonstrated using the prescribed criterion from Appendix H of ASME Section XI. Though Appendix H is for evaluating ferritic piping, the screening criteria are generic to fracture mechanics analysis and, hence, are applicable to the current evaluation.⁷ The details are presented in the enclosed technical report. The screening criteria demonstrate EPFM to be a valid method for determining the flaw instability behavior at the operating temperatures. The details of the EPFM method used in the evaluation are described in the enclosed technical report. The results from the EPFM method is presented in Table 2 and graphically shown in Figure 1.

Table 2: J-T Computations for ANO-1 RVH J-Groove Weld Remnant Crack Using EPFM (Guidance from Appendix K of ASME Section XI) Methodology.

Safety Factor (SF)	K_{Ip} SIF - Primary	K_{Ir} SIF - Residual	K_{Total} SIF - Total	r_p (Plastic Zone Size) (PZS)	a_c Corrected Crack Length For PZS	$\sqrt{(a_c/a)}$	K'_{Total} SIF- Total Corrected For PZS
	ksi/in			inches			ksi/in
S F= 1	3.7	90.7	94.4	0.131	1.631	1.043	98.4
*SF = 3, 1.5	11.1	136.1	147.2	0.319	1.819	1.101	162.0
SF = 2	7.4	181.4	188.8	0.525	2.025	1.162	219.4
SF = 3	11.1	272.1	283.2	1.182	2.682	1.337	378.7
SF = 3.5	13.0	317.5	330.4	1.609	3.109	1.440	475.6
SF = 4	14.8	362.8	377.6	2.101	3.601	1.549	585.1

⁵ See NUREG-0744, Volume 2, Revision 1; *Resolution of the Task A-11 Reactor Vessel Materials Toughness Safety Issue*; Appendices C-K; Division of Safety Technology, Office of Nuclear Reactor regulation, U. S. Nuclear Regulatory Commission, Washington, D. C. 20555; October 1982.

⁶ See "Advanced Fracture Mechanics," Melvin F. Kanninen and Carl H. Popelar; Oxford Press, Oxford, UK; 1985.

⁷ Ibid.

Table 2 (continued)

Safety Factor (SF)	K_{Ip}	K_{Ir}	K_{total}	K'_{total}	J'_{total}	T'	$J @$
	SIF - Primary	SIF - Residual	SIF - Total	SIF- Total Corrected For PZS	J-integral For Corrected Crack Length	Tearing Modulus For Corrected Crack Length	Instability
	ksi/in				in-kips/in ²		in-kips/in ²
SF = 1	3.7	90.7	94.4	98.4	0.315	0.916	4.4
*SF = 3, 1.5	11.1	136.1	147.2	162.0	0.853	2.483	4.4
SF = 2	7.4	181.4	188.8	219.4	1.564	4.551	4.4
SF = 3	11.1	272.1	283.2	378.7	4.660	13.559	4.4
SF = 3.5	13.0	317.5	330.4	475.6	7.353	21.392	4.4
SF = 4	14.8	362.8	377.6	585.1	11.125	32.367	4.4

- Appropriate Safety Factor case for ductile material: SF = 3 on primary, 1.5 on residual stress.
- The light green text represents results for much higher safety factors and shown for informative comparison purposes only.

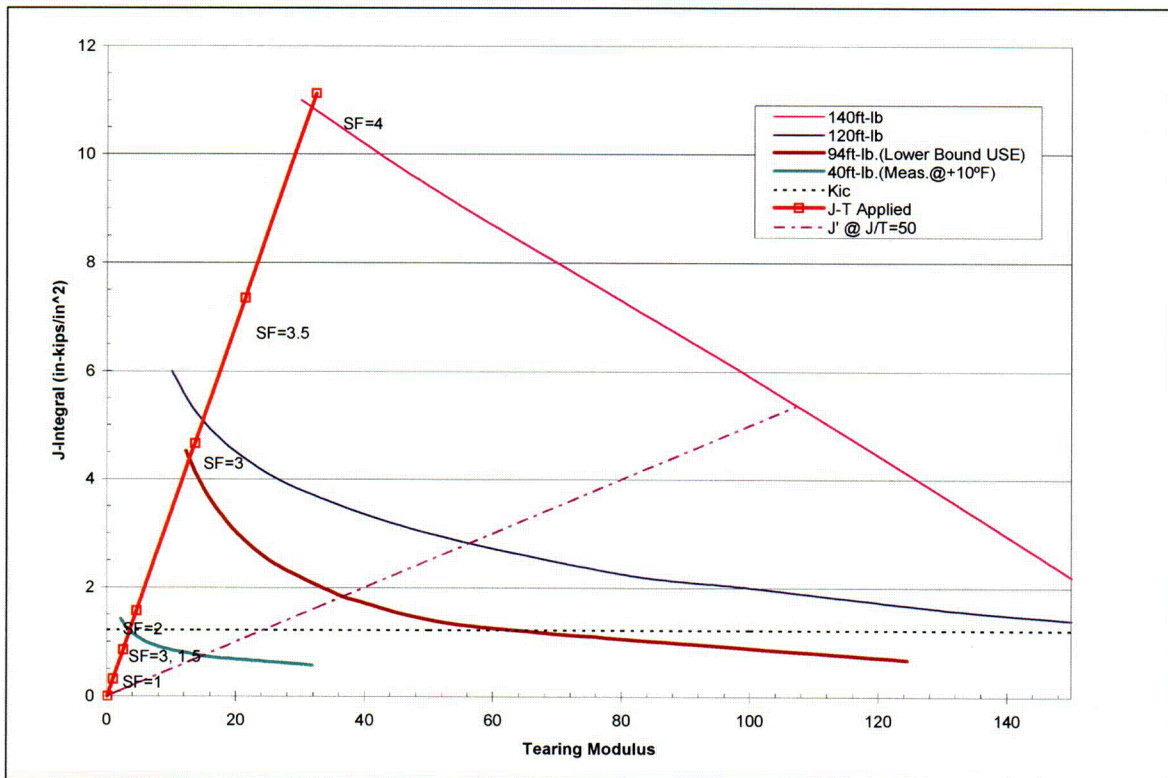


Figure 1: Results of the EPFM stability analysis for ANO-1 RPV head J-groove weld remnant crack. The applied line is the solid red colored line. The material toughness curves are shown to the right of this line. The intersection of the applied line and the material curves defines the instability point. The material curve for the current work is the 94 ft-lb curve. Two other USE curves (120 ft-lb and 140 ft-lb) are shown for information purposes. The lowest material curve is for the assumed 40 ft-lb absorbed energy obtained for the ANO-1 RPV head materials based on a single temperature test. This value for the absorbed energy is not representative of the actual materials USE, and hence is shown for a very worse case lower bound.

The results of the EPFM analysis demonstrate that proposed safety factors of 3.0 on primary stresses and 1.5 on residual stresses (indicated by the point labeled "SF = 3, 1.5" in Figure 1) provide adequate margin against flaw instability. From Table 2, the J value at instability for the ANO-1 RPV head material is found to be 4.4 in-kip/in², whereas the J value at the proposed safety factors is 0.853 in-kip/in². The margin against the instability of the postulated flaw (fully cracked J-prep) is 5.16 (4.4/0.853). Therefore, the proposed safety factors provide adequate assurance that the structural and leakage integrity of the RPV head at ANO-1 is maintained. The formulation of the proposed safety factors was based on a review of the pertinent sections of the ASME Code and supporting information from the literature. This effort is described in the enclosed technical report. Provided below is a summary of the information gleaned from this review, which supports the proposed safety factors.

The allowable SIF based on IWB-3613(b) is 63.2 ksi√in for an upper shelf fracture toughness of 200 ksi√in. As shown in Table 1 above, the applied SIFs are above the allowed value. The basis for the safety factor of "√10" in IWB-3613(b) can be found in Chapter 29 of the *ASME Companion Guide to the ASME Boiler and Pressure Vessel Code, Volume 2, "Section XI Flaw Acceptance Criteria and Evaluation Using Code Procedures"*. The Guide states:

The acceptance criteria of IWB-3611 on flaw size were developed with the original purpose of maintaining the design margins of Section III. It is well known that the nominal factor of safety for normal and upset conditions is 3. Consider the general relationship between the stress intensity factor and the stress and flaw size at failure based on linear-elastic fracture mechanics, as noted in the following equation:

$$K_{Ic} = \sigma \sqrt{\pi a}$$

where K_{Ic} = the fracture toughness.

It may, therefore, be deduced that a factor of safety of 3 on stress at failure is consistent with a factor of safety of 9 on flaw size. Code committees tend to prefer round numbers, so the value of 9 is rounded up to 10 to provide a safety factor slightly higher than the design safety factor.

Therefore, the safety factor on the SIF, based on the above equation, results in a value of √10. The design safety factor value of 3 was based on the ultimate tensile strength of the ferritic material thereby limiting the applied general primary membrane stress (P_m) to be less than or equal to one-third of the material ultimate strength.⁸

In addition, the design rules for Section III of the ASME Boiler and Pressure Vessel Code are defined for primary bending stress (P_b) and local primary membrane stress (P_L) to be lower than 1.5 S_m , which is approximately equal to the material yield strength. Further, the stress range when considering secondary stresses is increased by an additional factor of 2 to 3 S_m . This increase for local primary stresses then results in a nominal safety factor of 2 with consideration of bending and local stress effects. The limit on secondary stresses was included to prevent gross distortion of Code components.

⁸ See Chapter 6 of the *Companion Guide to the ASME Boiler and Pressure Vessel Code, Volume 1, "Subsection NB – Class 1 Components"*.

The aspect of using different safety factors based on loading type was recognized in Appendix G to ASME Section XI. Although this appendix is for “hypothetical flaw analysis” to ensure safety against non-ductile fracture, its applicability to the evaluation of flaws potentially left in the CRDM J-groove welds is appropriate. The current evaluation assumes that the entire J-groove weld (including the butter) is cracked, which is analogous to postulating a maximum worst-case hypothetical flaw. In particular the guidance provided in paragraph G-2222 (Consideration of Membrane and Bending Stresses) notes that, “Equation (1) of G-2215 requires modification to include the bending stresses which may be important contributors to the calculated K_I value at a point near a flange or nozzle.” Therefore, the controlling SIF equation, based on material toughness, was defined as:

$$K_{Ia} \geq 2 (K_{Im} + K_{Ib})_{Primary} + (K_{Im} + K_{Ib})_{Secondary}$$

where:

K_{Ia} = the available fracture toughness based on crack arrest for the corresponding crack tip temperature;

K_{Im} = the applied SIF due to membrane stress; and,

K_{Ib} = the applied SIF due to bending stress

In Appendix G, the distinction between primary and secondary stresses are recognized by using a safety factor of 2 on primary stresses and a safety factor of 1 on secondary stresses.

The safety factor considerations in the Code (Section III and Appendix G of Section XI) are based on the through-wall stress distribution, which is also the consideration for IWB-3600 of ASME Section XI. However, the safety factor presented in IWB-3613(b) considers the same safety factor for all stresses. This results in an overly conservative allowable SIF when the predominant loading mechanism is highly localized and due to residual stresses.

A more reasonable approach would be to utilize the philosophy of Appendix G and the safety factors utilized in Section III. This approach would result in the governing equation for SIF as:

$$K_{Ia} \geq 3.0 (K_{Im} + K_{Ib})_{Primary} + 1.5 (K_{Im} + K_{Ib})_{Secondary \text{ (or Residual)}}$$

In the above equation, the primary stresses would be those from operating pressure, which are the only non-displacement limited load on the top head. The secondary stresses would be those due to local structural discontinuity effects and thermal gradients. The safety factors applied are determined by multiplying those in Appendix G by a factor of 1.5. In this manner, the appropriate safety margin against non-ductile fracture would be maintained in a manner similar to that prescribed by Appendix G but with a higher safety factor.

The information presented in the enclosed technical report and summarized above shows that there is significant margin against flaw instability using the proposed acceptance criteria. In addition, the overall approach is conservative in that:

1. The fracture mechanics evaluation is based on a hypothetical flaw that is assumed to exist in the entire J-groove.
2. The evaluations based on EPFM methods demonstrate that sufficiently high margin against flaw instability exists.

3. The safety factors of 3.0 on primary stresses and 1.5 on residual stresses for the evaluation of the remnant J-groove weld flaw, postulated as a fully cracked J-prep, has been demonstrated to provide adequate safety (by a factor of 5.16) against flaw instability.

In order to ensure the completeness of the evaluation, the stress distributions resulting from the impact of the new repair weld joining the nozzle to the RPV head at an elevation of approximately 2.0 inches above the top of the uphill J-groove weld, were compared. The comparison was between the stress distributions in the J-groove weld vicinity just prior to the installation of the new repair weld to that from just after completion of the new repair weld. This comparison is documented in the enclosed technical report. The comparison shows that there is a decrease in the magnitude of the hoop stress distribution, in the vicinity of the J-groove weld, upon completion of the new repair weld. However, in the stress analysis that was used for the LEFM analysis to determine the SIF, this reduction in the hoop stress was not considered. Hence, a more conservative stress distribution, which would lead to a higher SIF, was used. Since, the applied J in the EPFM analysis was derived from the SIF from the LEFM analysis, the applied J was also conservatively higher than that expected from the use of a more realistic stress distribution. This finding shows that there is an added conservatism in the result from the EPFM analysis. Therefore, it is concluded that the proposed safety factors of 3.0 on primary stresses and 1.5 on residual stresses provide adequate safety against flaw instability and are in accordance with the safety factors for design prescribed in ASME Section III.

Therefore, the analysis demonstrates that the structural and leakage integrity of the ANO-1 RPV head is maintained for the remaining life of the head (one operating cycle).

B. Examining the Repair Weld

Industry experience gained from earlier repairs of RPV head nozzles indicates that removal and repair of the defective portions of the original J-groove partial penetration welds were time consuming and radiation dose intensive. The prior repairs indicated that more automated repair methods were needed to reduce radiation dose to repair personnel. For the present ANO-1 repairs, a remote semi-automated repair method will be used for each of the subject nozzles. Using a remote tool from above the RPV head, each of the nozzles subject to this repair will first receive a roll expansion into the RPV head base material to insure that the nozzle will not move during subsequent repair operations. Second, a semi-automated machining tool from underneath the RPV head will remove the lower portion of the nozzle to a depth above the existing J-groove partial penetration weld. This operation will sever the existing J-groove partial penetration weld from the subject RPV head nozzles. Third, a semi-automated weld tool, utilizing the machine GTAW process, will then be used to install a new Alloy 690 pressure boundary weld between the shortened nozzle and the inside bore of the RPV head base material (see Figures 2 and 3). It was intended, as a part of the new repair methodology and to reduce radiation dose to repair personnel that the original J-groove partial penetration welds would be left in place. These welds will no longer function as pressure boundary RPV head nozzle to RPV head welds. However, the possible existence of cracks in these welds mandates that the flaw growth potential be evaluated.

In the case of the RPV head nozzle inside diameter (ID) temper bead repair, the term "anomaly" is applied to the unusual solidification patterns that result along the low alloy steel / Alloy 600/Filler Metal 52 interface of the repair weld. The anomalies originate along the low alloy steel (RPV head) to Alloy 600 (original nozzle) interface where melting occurs and generally extend back towards the center of the weld bead. These anomalies are typical for

welds that involve a "lap joint" type interface, such as typical partial penetration weld geometries, in the weld joint design. Cross sections of nickel alloy welds made utilizing similar joint designs with Alloy 600 base materials and Alloy 82 filler metals have exhibited these phenomena consistently.

This phenomenon is compounded by the different solidification rates for the base materials and weld metal used in performing the repair. Other suspected factors in the anomaly occurrence are the size of the interface gap, gap cleanliness and position of the welding arc relative to the edge of the interface. The molten weld puddle simply freezes back to each side of the interface and follows the interface into the weld as solidification of the weld puddle take place. Weld root anomalies have been observed on several mockups with configurations simulating the repair weld. UT methods have been developed based on the characteristics of this anomaly so that verification to the prescribed acceptance criteria can be performed. The defect is treated like a crack, which is worst case. Two types of flaws are common in this area. The first is localized melting away of the feathered end of the beveled nozzle weld prep leaving occasional small voids. The second type flaw is caused due to an inherent problem during solidification of high Ni-Cr alloys in the presence of a notch such as a partial penetration weld. This type of flaw is in fact often called a "solidification anomaly" to differentiate it from what it is not – a crack.

IWA-4170 mandates that the repair design meets the original construction code or the adopted ASME Section III Code. As noted, the 1989 ASME Section III code has been adopted for qualification of the described repairs. Subsection NB-5330(b) stipulates that no lack of fusion area be present in the weld. A fracture mechanics analysis was performed to demonstrate compliance with Section XI of the ASME Code, for operating with the postulated weld anomaly described above.⁹ The anomaly was modeled as a 0.1 inch "crack-like" defect, 360 degrees around the circumference at the "triple point" location. Full-size mockups using coupons from the Midland RPV head were metallographically evaluated. Both flaw types were occasionally found as expected and were less than the analyzed maximum allowed of 0.100 inch.¹⁰

Based on the fact that this anomaly is predictable as discussed herein, the anomaly can be detected by UT within the prescribed acceptance criteria and evaluated for fatigue and flaw growth using applicable ASME Sections III and XI methods. Therefore, the intent of the ASME Codes will be met. The ASME Section III analysis conservatively assumes a reduction in weld area (along the new weld-to-ferritic steel penetration fusion line) due to the anomaly and the ASME Section XI analysis assumes the anomaly is a crack-like defect.

Postulated flaws could be oriented within the anomaly such that there are two possible flaw propagation paths, as discussed below.

Path 1:

Flaw propagation path 1 traverses the RPV head tube wall thickness from the outside diameter (OD) of the tube to the ID of the tube. This is the shortest path through the component wall, passing through the new Alloy 690 weld material. However, Alloy 600 tube material properties or equivalent are used to ensure that another potential path

⁹ See ANO Calculations 86-E-0074-160 and 86-E-0074-161 submitted to the NRC via Entergy letter CNRO-2002-00054 dated November 26, 2002.

¹⁰ ANO Calculation 86-E-0074-160, page 2 and ANO Calculation 86-E-0074-161, page 4

through the heat affected zone (HAZ) between the new repair weld and the Alloy 600 tube material is bounded.¹¹

For completeness, two types of flaws are postulated at the outside surface of the tube. A 360 degree continuous circumferential flaw, lying in a horizontal plane, is considered to be a conservative representation of crack-like defects that may exist in the weld anomaly. This flaw is subjected to axial stresses in the tube. An axially oriented semi-circular outside surface flaw is also considered since it would lie in a plane normal to the higher circumferential stresses. Both of these flaws would propagate toward the inside surface of the tube.¹²

Path 2:

Flaw propagation path 2 runs down the outside surface of the repair weld between the weld and RPV head. A semi-circular cylindrically oriented flaw is postulated to lie along this interface, subjected to radial stresses with respect to the tube. This flaw may propagate through either the new Alloy 690 weld material or the low alloy steel RPV head material.¹³

The result of the analysis demonstrated that a 0.10-inch weld anomaly is acceptable for 25 years, which is beyond 2005 when the ANO-1 RPV head is scheduled to be replaced.¹⁴ Residual stresses and stresses due to operation were considered. Significant fracture toughness margins were expected for both of the flaw propagation paths considered in the analysis. The minimum calculated fracture toughness margins were required to be greater than the required margin of $\sqrt{10}$ per ASME Section XI IWB-3612. Based on similar analysis, fatigue crack growth was expected to be minimal. The maximum final flaw size was small considering both flaw propagation paths. A limit load analysis was also performed considering the ductile Alloy 600/Alloy 690 materials along flaw propagation path 1. The analysis was required to show limit load margins for normal/upset conditions and emergency/faulted conditions greater than the required margins of 3.0 and 1.5 for normal/upset conditions and emergency/faulted conditions, respectively, per ASME Section XI, IWB-3642.¹⁵

Acceptance of the repair weld is based on this evaluation in accordance with ASME Section XI and demonstrated that for the intended service life of the repair, the fatigue crack growth is acceptable and the crack-like indications remain stable. These two findings satisfy the Section XI criteria but do not include considerations of stress corrosion cracking such as PWSCC. However, since the crack-like indications in the weld triple point anomaly are not exposed to the primary coolant and the air environment is benign for the materials at the triple point, the time-dependent crack growth from PWSCC is not applicable.

Eliminating the weld triple point anomaly requires use of an entirely different process than that proposed for use on ANO-1. The only qualified method currently available would involve extensive manual welding that would result in radiation doses estimated to be in excess of 30 REM per nozzle as compared to the 5 REM estimated for each nozzle repaired by the

¹¹ ANO Calculation 86-E-0074-161, page 7

¹² Ibid.

¹³ Ibid.

¹⁴ ANO Calculation 86-E-0074-161, page 38

¹⁵ ANO Calculation 86-E-0074-161, pages 22, 23, and 38

proposed process. Compliance with the specified Code requirements would result in excessive radiation exposure.

V. Duration of the Proposed Alternative

Entergy plans to replace the ANO-1 RPV head during Refueling Outage 1R19, which is scheduled to begin during the fall of 2005. Therefore, this request applies to:

- The previous operating cycle for the six (6) nozzles repaired in 1R17 using the Framatome technique, which was approved via alternative ANO1-R&R-004¹⁶, and
- Upcoming Operating Cycle 19 for any of the 69 RPV head penetration nozzles that may be repaired during 1R18.

For the upcoming Operating Cycle 19, Entergy has evaluated the need to employ water jet conditioning and has determined such activities are not required. Entergy has performed an evaluation to determine the time for a postulated crack to grow 75% through-wall in the Alloy 600 nozzle material above the repair weld without employing water jet conditioning, as documented in Engineering Report M-EP-2004-002, Rev. 0.

The evaluation considers RPV head nozzles in the as-repaired condition and encompasses initiation and crack growth due to primary water stress corrosion cracking (PWSCC). This evaluation found that nozzle axial stresses are considerably lower than nozzle hoop stresses. Because of this, the likelihood of axial cracking is greater than the likelihood of circumferential cracking; therefore, only axial crack conditions were analyzed.

The analysis indicates that a crack will not grow to 75% through-wall in a time period of four years. This estimate is based on the following assumptions:

1. After PT and UT examination of the repaired ID surface, an undetected axial crack 0.157 inch long and 0.0679 inch deep (11% wall thickness) is assumed present.¹⁷
2. The crack growth rate under operating conditions was determined using the MRP-55 recommended curve modified for a crack growth amplitude (α) that represents B&W material data.¹⁸
3. The minimum wall thickness of the CRDM nozzle repair is 0.6175.¹⁹
4. Water jet conditioning is not applied.

Since Entergy plans to replace the ANO-1 RPV head during 1R19, which is prior to the end of four years, water jet conditioning is not necessary.

Given these expected results, the proposed inspection schedules given above, and the planned replacement date for the ANO-1 RPV head, Entergy believes the proposed alternatives to the ASME Code requirements are justified. The proposed alternatives are applicable to the repairs and examinations after repair to any ANO-1 RPV head nozzle.

¹⁶ Request for Alternative ANO1-R&R-004 (TAC No. MB6599) was approved by the NRC in a letter dated November 25, 2003.

¹⁷ Engineering Report M-EP-2004-002, Rev. 0, Attachment 2 of Appendix C, page 2 of 17

¹⁸ Engineering Report M-EP-2004-002, Rev. 0, Appendix B

¹⁹ Engineering Report M-EP-2004-002, Rev. 0, Appendix A gives nozzle ID and OD dimensions.

VI. Implementation Schedule

This request will be implemented during upcoming refueling outage 1R18, which is scheduled to begin during the second quarter of 2004. Entergy plans to replace the ANO-1 RPV head during Refueling Outage 1R19, which is scheduled to begin during the fall of 2005.

VII. Conclusions

10CFR50.55a(a)(3) states:

Proposed alternatives to the requirements of (c), (d), (e), (f), (g), and (h) of this section or portions thereof may be used when authorized by the Director of the Office of Nuclear Reactor Regulation. The applicant shall demonstrate that:

- (i) The proposed alternatives would provide an acceptable level of quality and safety, or
- (ii) Compliance with the specified requirements of this section would result in hardship or unusual difficulty without a compensating increase in the level of quality and safety.

Entergy believes that the proposed alternative provides an acceptable level of quality and safety because, as discussed in Section IV, above:

- Leaving a remnant of the original J-groove weld in place has been analyzed and shown to pose no adverse effect on plant operations.
- Although the SIF of a postulated crack in the J-groove weld remnant does not meet ASME Section XI requirements using a safety factor of $\sqrt{10}$. Using safety factors of 3 (primary stresses) and 1.5 [secondary stresses (which include residual stresses)], which is commensurate with ASME Section III design requirements, the analysis demonstrates that the structural and leakage integrity of the ANO-1 RPV head is maintained for the remaining life of the head (one operating cycle).
- Analysis has been performed demonstrating that a 0.1-inch weld anomaly in a new repair weld is acceptable for four years, which is beyond 2005 when the ANO-1 RPV head is to be replaced.

Therefore, Entergy requests that the NRC staff authorize this request pursuant to 10 CFR 50.55a(a)(3)(i).

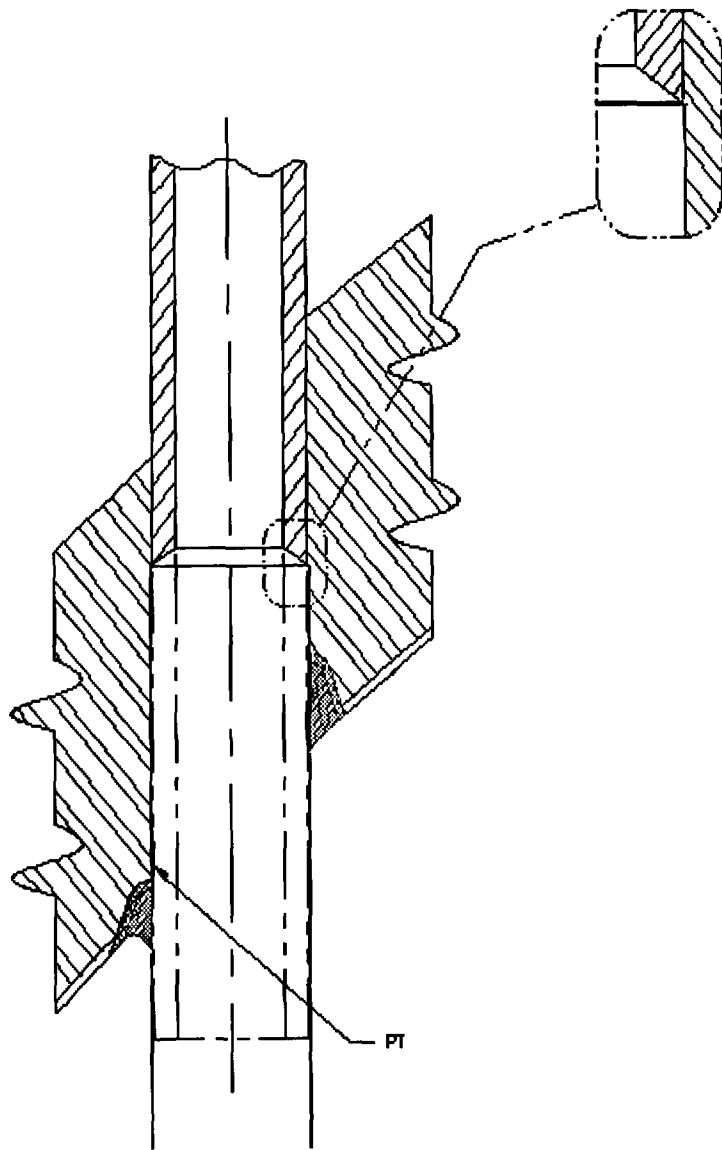


FIGURE 2
New ANO-1 RPV Head Nozzle

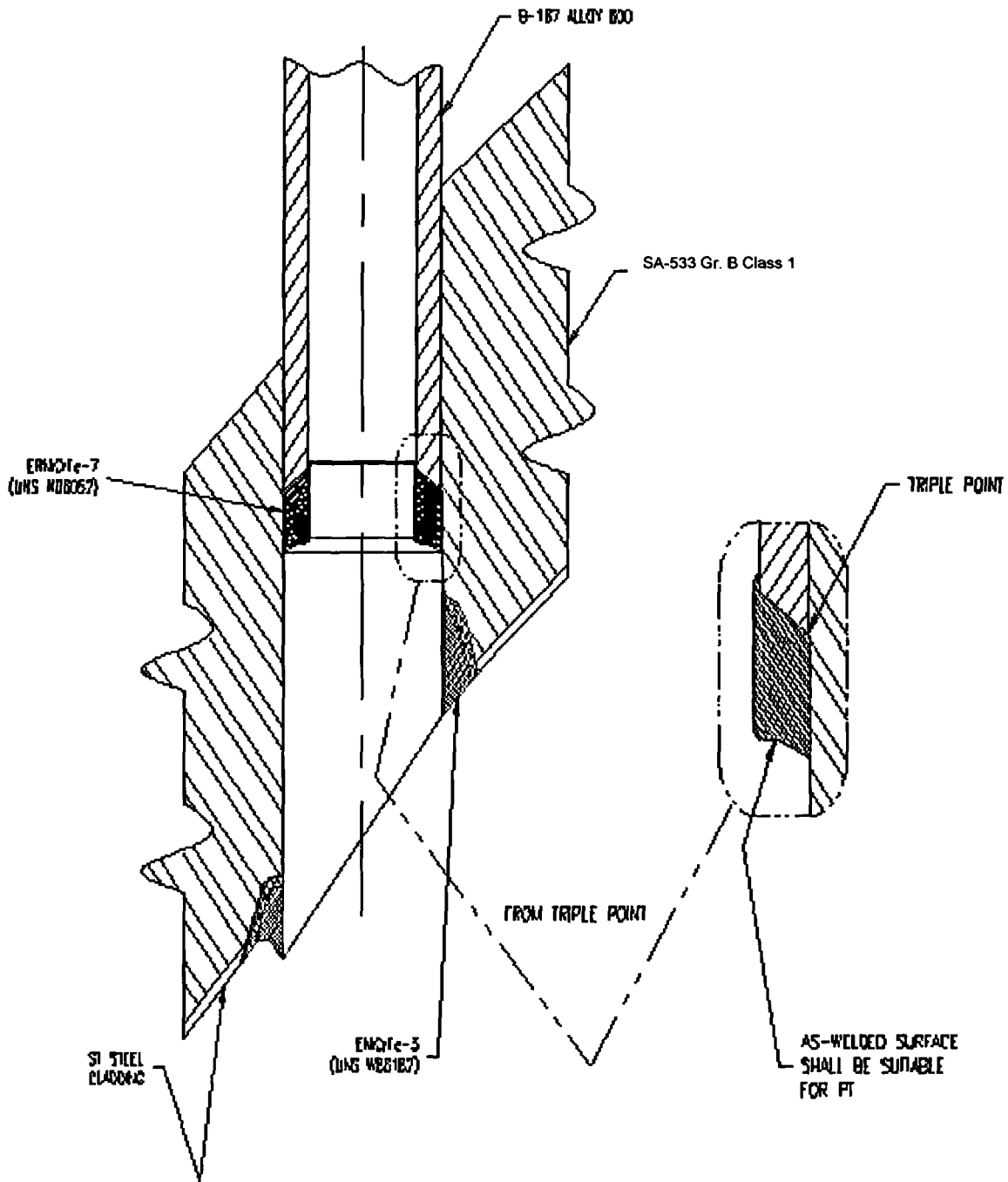


FIGURE 3
ANO-1 New RPV Head Pressure Boundary Welds

ENCLOSURE 3

CNRO-2004-00026

**TECHNICAL REPORT SUPPORTING
ANO1-R&R-006, Rev. 0**

Technical Report to Support Relief Request ANO1-R&R-006

Introduction

The review of the fracture mechanics analysis for the J-groove weld remnant, documented in [1], indicates that the analysis was not sufficiently rigorous. Two concerns were identified, which led to the conclusion that the analysis (presented in Reference 1) was not an accurate representation of the prevailing conditions of the J-groove weld remnant. These concerns were:

Concern 1: The stress intensity factor (SIF) equation, used in the analysis of the J-groove weld flaw, in Reference 1 was obtained from Reference 2. The formulation, Figure 1, was a combination of two influence function solutions. The two solutions used to derive a solution [2] for the corner flaw in a nozzle were:

- a) A semi-circular crack on a half-space (upper left in Figure 1); and,
- b) A quarter-circular crack in a quarter-space (upper right in Figure 1).

The derivation for the corner crack for a nozzle consisted of averaging the coefficients from the two equations for the two other crack models described above. The coefficients for the nozzle corner flaw are shown in the lower right sketch of Figure 1. The averaging of the two coefficients for the linear term (A_1) appears to be in error. The average of the coefficients from the two base models results in a value of 0.511 for the resulting coefficient, whereas the value in the equation is 0.537.

The publication, cited in Reference 2, was published at the request of the ASME Nuclear Codes and Standards Department to provide the information to utility members. The foreword to this publication clearly states that; "*The solutions provided herein are for information only*". Furthermore, the reference cited for this formulation is a personal communication between two individuals. There is no cited reference that provides an analytical basis for the formulation.

The equation, though published in the Electric Power Research Institute (EPRI) document, does not have the necessary confirming documentation to evaluate the validity of its application. Furthermore, the crack geometry, which has a quarter-circular shape, does not define the J-groove weld geometry properly. The J-groove weld geometry is a distorted quarter-ellipse.

Thus, Entergy believes the use of this model is improper because:

- a) There is no documented validation of the model; and,
- b) The geometry does not adequately represent a J-groove weld.

Concern 2: In the analysis presented in Reference 1 the residual stress distribution from the J-groove welding process was not explicitly considered as an applied stress. Instead, the residual stress profile (for an un-cracked J-groove weld) was used to define the initial flaw size. The justification provided in Reference 1 states in part:

"Although at shutdown, the residual hoop stress in the weld region is high, above 60,000 psi (Figures 5 and 8); the stresses decrease to zero just beyond the butter region and are compressive in the head. These residual stresses would be relieved as the crack propagates through the weld and butter and a short distance into the head.

Technical Report to Support Relief Request ANO1-R&R-006

Deeper cracks would then experience only the compressive residual stress ahead of the crack tip. It can be seen from Figure 8 and Table 4 that the residual stresses are compressive at some distance less than 0.436" into the head. The depth of the initial flaw size will therefore be increased by this amount so that residual stresses need not be considered in the present flaw evaluation".

The evaluation, which used an influence function (weight function) method, is predicated on the following bases [3]:

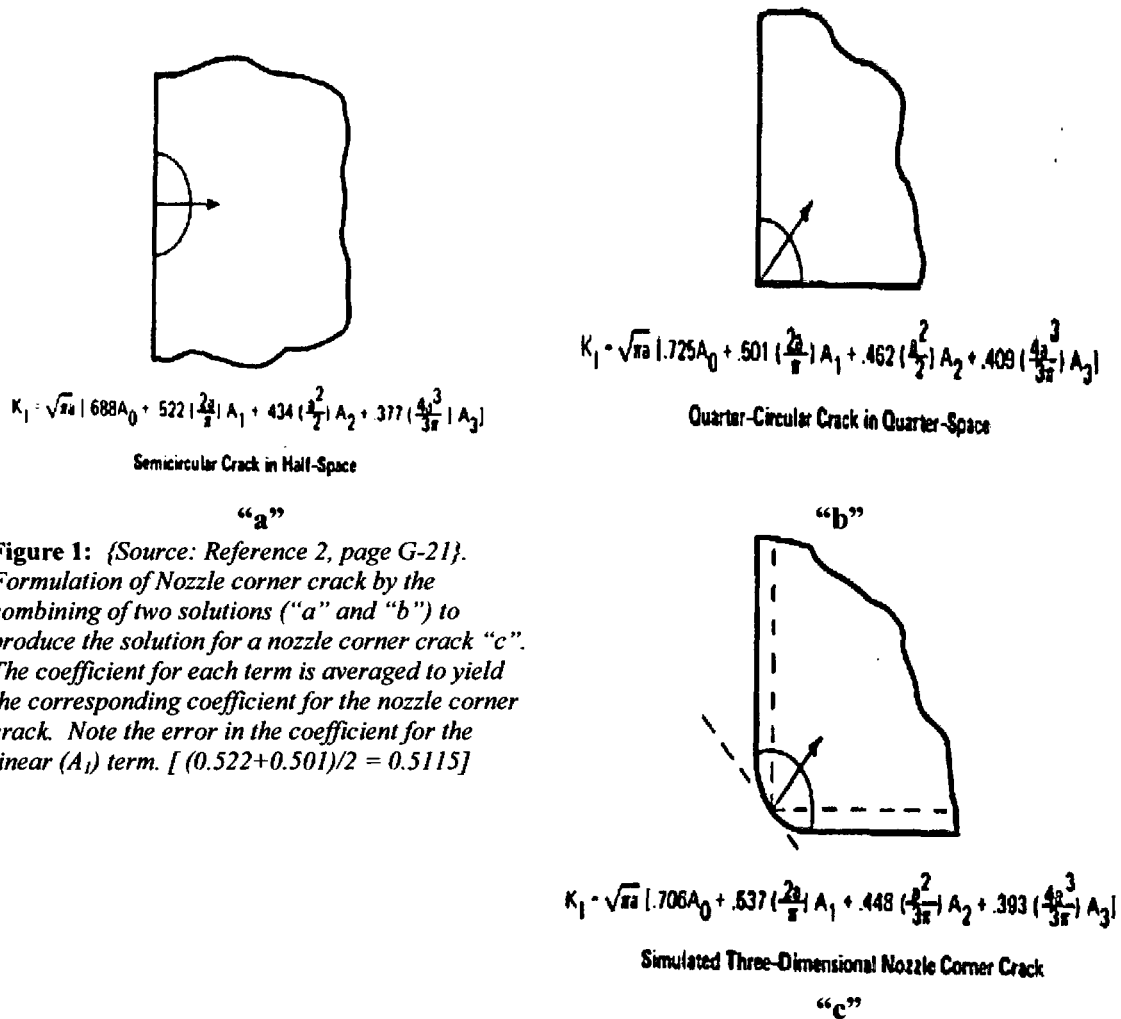
- a) The integration to obtain the weight function is carried out over the depth of the crack "a", and the stress distribution $\sigma(x)$ across the plane of the crack in the uncracked body.
- b) The stress distribution when integrated over the depth of the crack is the "force system" with which the stress intensity factor is associated.
- c) The "force system" and, therefore, the stress distribution can be arbitrary across the plane of the crack.
- d) Only the stress distribution that is bounded by the cracked region is considered in the analysis. The stress distribution ahead of the crack front is of no consequence.

Contrary to the basis of the analytical method (influence function/weight function) that required the stress distribution in the cracked region be considered, the justification provided in Reference 1, and cited above, ignores the contribution from residual stress distribution. Therefore, the assumption made in Reference 1 violates the basis of the method.

Thus, Entergy believes that ignoring the residual stress distribution is improper because:

- a) It violates the basis of the method of analysis; and,
- b) The results would be non-conservative since the crack face is not loaded by the force from residual stresses in the cracked region.

Technical Report to Support Relief Request ANO1-R&R-006



$$K_1 = \sqrt{\pi a} \left[688A_0 + 522 \left(\frac{2a}{r} \right) A_1 + 434 \left(\frac{a^2}{r^2} \right) A_2 + 377 \left(\frac{4a^3}{3r^3} \right) A_3 \right]$$

Semicircular Crack in Half-Space

$$K_1 = \sqrt{\pi a} \left[725A_0 + 501 \left(\frac{2a}{r} \right) A_1 + 462 \left(\frac{a^2}{r^2} \right) A_2 + 409 \left(\frac{4a^3}{3r^3} \right) A_3 \right]$$

Quarter-Circular Crack in Quarter-Space

$$K_1 = \sqrt{\pi a} \left[706A_0 + 537 \left(\frac{2a}{r} \right) A_1 + 448 \left(\frac{a^2}{r^2} \right) A_2 + 393 \left(\frac{4a^3}{3r^3} \right) A_3 \right]$$

Simulated Three-Dimensional Nozzle Corner Crack

Figure 1: {Source: Reference 2, page G-21}.
 Formulation of Nozzle corner crack by the combining of two solutions (“a” and “b”) to produce the solution for a nozzle corner crack “c”. The coefficient for each term is averaged to yield the corresponding coefficient for the nozzle corner crack. Note the error in the coefficient for the linear (A_1) term. $[(0.522+0.501)/2 = 0.5115]$

In order to resolve the concern in a succinct manner, detailed finite element analyses for the residual stresses and fracture mechanics were undertaken. These analyses were designed to ensure that both the geometry and the loading conditions were accurately represented.

The flaw geometry with respect to the uphill J-groove weld is presented in Figure 2.

Technical Report to Support Relief Request ANO1-R&R-006

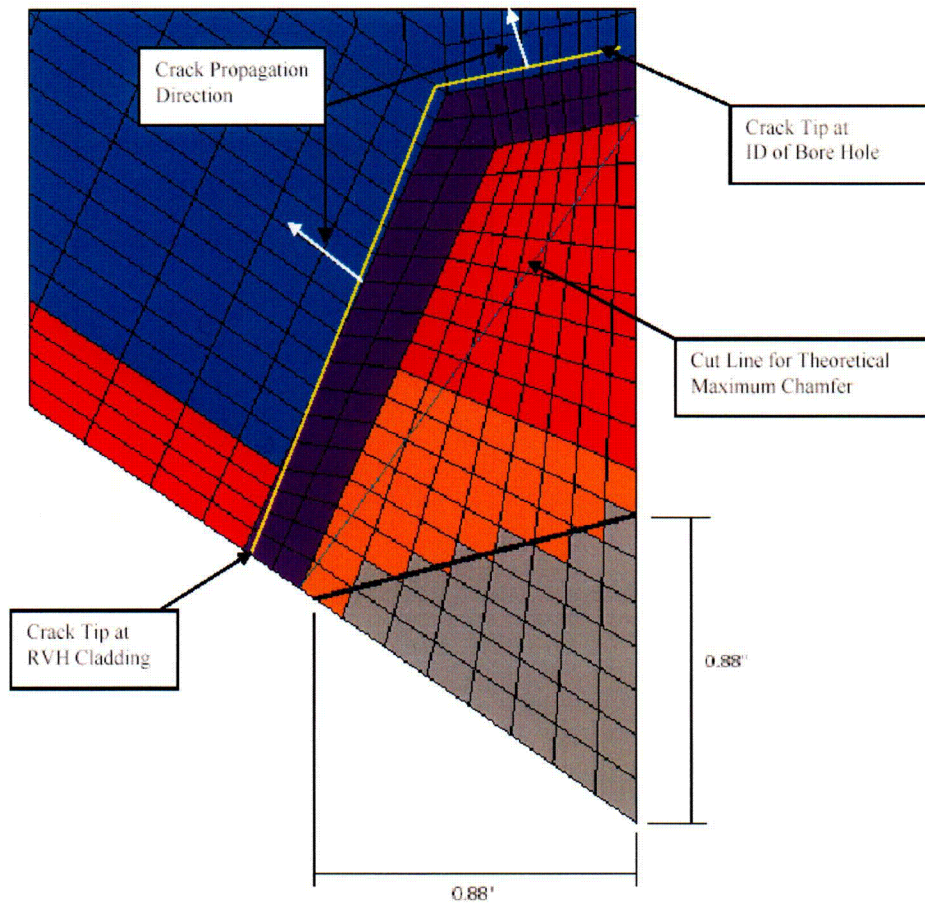


Figure 2: The crack flaw geometry with respect to the J-groove weld on the uphill side. The joint configuration is as follows:

- 1) The J-groove weld is the trapezoid shown in red, light brown and grey color.
- 2) The purple color bounding the J-groove weld is the buttering layer.
- 3) The light blue color beyond the buttering layer is the low alloy steel reactor vessel head (RVH).
- 4) The magenta color strip is the stainless steel cladding on the reactor vessel head (RVH) inside diameter (ID) surface.

The flaw geometry is defined as follows:

- 1) The flaw tip (crack front) is along the interface between the buttering layer and the RVH (shown by yellow line)
- 2) Two flaw regions are marked; a) the design maximum chamfer case, shown by the colored elements in red, light brown and the buttering in purple (note the chamfer size of 0.88 inch), and b) the maximum chamfer line shown in light turquoise color (the crack is the entire J-weld prep. Note, the design minimum chamfer size of 0.63 inch is not shown and would be of a size in-between the no chamfer and the design maximum chamfer geometry.
- 3) The no chamfer flaw would be composed of the grey, light brown, red and the purple colored elements.
- 4) The crack propagation direction is shown by white arrows.

CO2

Technical Report to Support Relief Request ANO1-R&R-006

The installation of the Framatome Technologies incorporated (FTI) repair design requires the counterboring of the existing nozzle followed by welding the cut nozzle to the reactor vessel head (RVH). The final step in this repair process is the machining of the corner of the remnant J-groove weld to create a chamfer. Since the J-groove weld cannot be inspected by available (qualified) non-destructive examination methods, the weld has to be assumed to be completely cracked (J-groove weld and butter). The J-groove weld butter has an interface with the low alloy steel RVH hence, the assumed flaw has to be evaluated to ascertain the propensity for brittle fracture of the low alloy steel RVH.

Figure 2 is a sketch of the joint geometry at the uphill location. The J-groove weld prep is approximated by two lines that intersect at the knee of the weld prep. In actual practice the J-groove contour is a smooth curve. This approximation is made to simplify the modeling effort and is not expected to significantly impact the results. It is important to note that the theoretical maximum chamfer case is an assumed maximum for the purpose of this analysis. This theoretical maximum chamfer case was included to evaluate the SIF behavior with respect to the chamfer size. Thus, evaluating a full complement, using the "no chamfer" and the "theoretical maximum chamfer" to bracket the two design chamfer sizes, would provide sufficient information for a rational evaluation. Figure 2 shows the finite element mesh that was used in the stress analysis. It should be noted that the finite element mesh used in the fracture mechanics analysis is more refined in the crack region. In this figure the crack front along the buttering layer and the low alloy steel RVH is shown by the yellow line. The crack propagation direction shown assumes a self-similar crack profile and hence, the propagation direction is shown as being orthogonal to the crack front. The crack region for the three chamfer designs is also shown. The bore ID is to the right of the sketch. This figure shows that the assumed crack encompasses the entire J-groove weld including the buttering layer. Since both the J-groove weld and the buttering layer material are made from Inconel Alloy 82/182 (similar to Inconel Alloy 600) it is considered susceptible to primary water stress corrosion cracking (PWSCC). Therefore, the entire weld is assumed to be cracked by a PWSCC mechanism. The low alloy steel RVH material is very resistant to PWSCC under the electrochemical conditions prevailing in the reactor coolant system and is not assumed to be cracked by the PWSCC mechanism. Crack growth into the low alloy steel RVH material would be by a fatigue mechanism.

In the following sections a brief description of the models, the analysis method, results from the analysis and a discussion on the application of an adequate safety factor to ensure against non-ductile failure are presented.

Technical Report to Support Relief Request ANO1-R&R-006

Residual Stress Analysis

As-Built Analysis

The detailed finite element analysis for residual stress determination [4] showed that the hoop and axial stresses tend to increase with the increased penetration angle of the nozzle axis with respect to the RVH. This was found to be the case for the uphill side of the J-groove weld where the nozzle stresses were the highest. In order to develop a bounding analysis, the outermost penetration angle (38.5°) was selected. Since the analyses in Reference 4 also shows that the residual stresses increase with nozzle material yield strength, the analysis was performed with the highest yield strength. In this manner, an upper bound residual stress distribution is obtained. The modeling for determining the residual stresses in the as-built condition [5] was as follows:

- 1) The finite element mesh consisted of 3-dimensional solid (brick) elements. Four elements were used to model the tube wall with similar refinement carried to the attaching J-weld.
- 2) The control rod drive mechanism (CRDM) tube material was modeled with a monotonic stress-strain curve. The highest yield strength from the nozzle material bounded by the nozzle group was used. This yield strength was referenced to the room temperature yield strength of the stress-strain curve described in Reference 5. The temperature dependent stress-strain curves were obtained by indexing the temperature dependent drop of yield strength.
- 3) The weld material was modeled as elastic-perfectly plastic for the weld simulation. This approximation is considered reasonable since most of the plastic strain in the weld metal occurs at high temperatures where metals do not work-harden significantly [6]. The temperature in the weld is high during the welding process. Once the weld begins to cool, the temperatures in the weld at which strain hardening would persist are of limited duration [6]. This was borne out by the comparison between the analysis based residual stress distribution and that obtained from experiments [7].
- 4) A simulation of the post weld heat treatment (PWHT) was performed after the buttering layer was applied by welding.
- 5) The J-groove weld is simulated by two passes based on studies presented in Reference 5.
- 6) After completing the j-groove weld, a simulated hydro-test load step is applied to the model. The hydro-test step followed the fabrication practice.

Technical Report to Support Relief Request ANO1-R&R-006

- 7) The model is then subjected to a normal operating schedule of normal heat up to steady state conditions at operating pressure. Upon reaching steady state conditions the normal cooldown cycle is simulated to achieve ambient conditions. At this time the repair models are executed.

The stress contours for the outermost nozzle obtained from the finite element analysis are presented in Figure 3. The stress contour color scheme is as follows:

Dark Navy blue	from Minimum (Compression) to -10 ksi
Royal blue	from -10 to 0 ksi
Light blue	from 0 to 10 ksi
Light green	from 10 to 20 ksi
Green	from 20 to 30 ksi
Yellow green	from 30 to 40 ksi
Yellow	from 40 to 50 ksi
Red	from 50 to 100 ksi

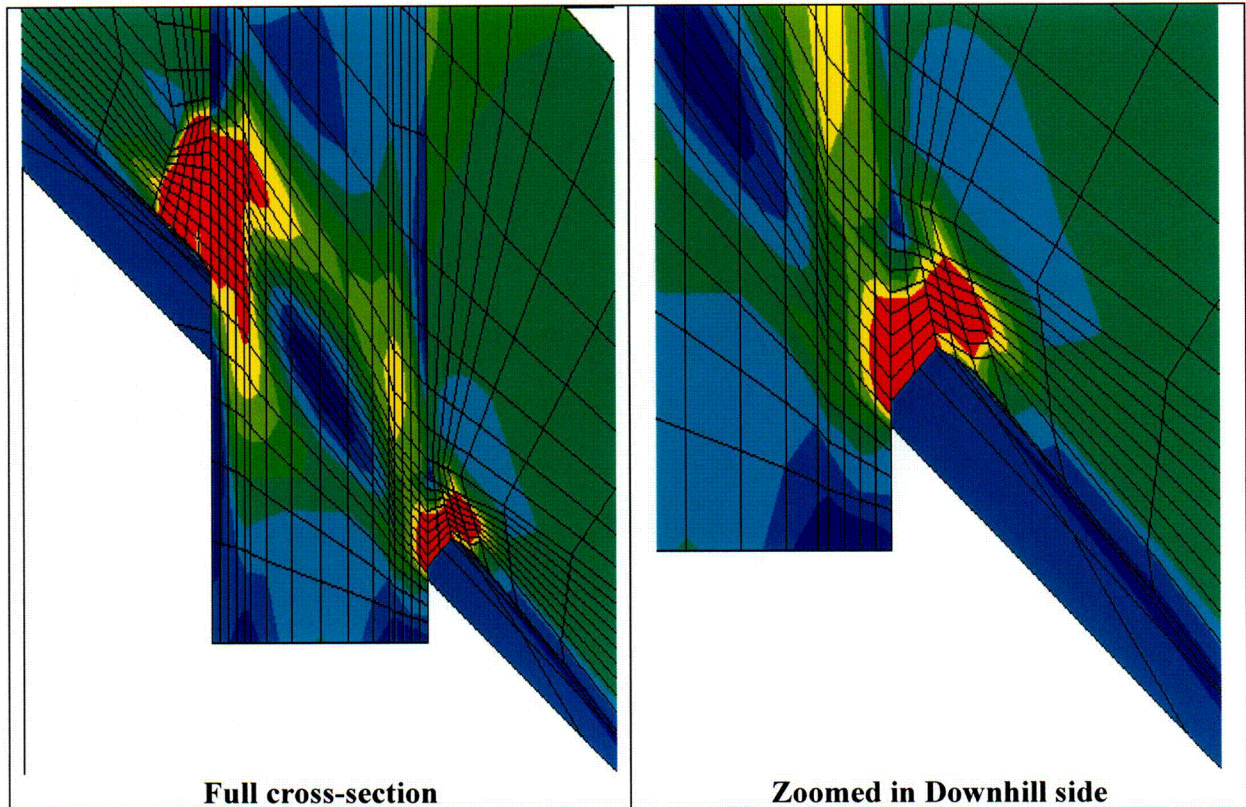


Figure 3: Hoop stress contours for the 38.5° nozzle. High tensile stresses occur in the weld and adjacent tube material.

C03

Technical Report to Support Relief Request ANO1-R&R-006

Chamfer Repair Analysis

The repair of the degraded nozzle was accomplished by counterboring the existing nozzle to an elevation that was approximately two (2.0) inches above the top of the uphill weld. The remaining nozzle was secured by roller expansion, which was followed by welding the nozzle end to the RVH by a temper bead welding process. The final repair process involved installing a chamfer on the J-groove weld remnant. This chamfer was made to reduce the J-groove weld size since the fracture mechanics analysis postulates that the entire J-groove weld (including the butter) is cracked. The removal of a portion of the J-groove weld is expected to reduce the flaw size sufficiently such that the stress intensity factor (SIF), based on the reduced flaw size and anticipated loading, is below the allowable limit specified in ASME Code Section XI paragraph IWB-3613(b) [8].

The chamfer design considered in the analysis was based on the design chamfer sizes [9] for the outer most penetration. Two additional cases, a no chamfer and a maximum theoretical chamfer, were evaluated to provide a complete set such that a better correlation between the SIF as a function of chamfer size could be developed. Therefore, the analysis was performed for four J-groove weld remnants, as follows (see Figure 2):

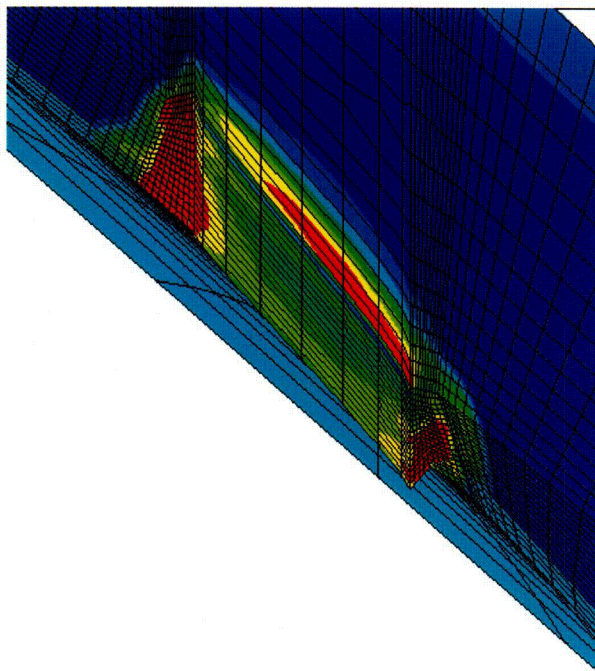
- 1) No chamfer, J-groove weld left as-is after counterboring.
- 2) Design minimum chamfer of 0.63 inch. This is the side of an equilateral right angle triangle at the corner of the remnant J-groove weld and is located on the uphill side. The contour is followed to the downhill side as specified in Reference 9.
- 3) Design maximum chamfer of 0.88 inch. This is the side of an equilateral right angle triangle at the corner of the remnant J-groove weld and is located on the uphill side. The contour is followed to the downhill side as specified in Reference 9.
- 4) A theoretical maximum chamfer based on a diagonal connecting the bottom of the buttering weld from the RVH bore to the inside of the buttering on the RVH cladding at both the uphill and downhill locations. The chamfer was swept from the uphill to the downhill to obtain the chamfer at intermediate locations in the finite element model.

The residual stresses data for the as-chamfered condition was saved. The model was then subjected to a normal heat-up and steady state sequence. Transient analysis was performed for the following transients:

- 1) Normal heat-up and cooldown.
- 2) Reactor trip at full power (normal and upset condition).
- 3) Inadvertent rod withdrawal (Accident condition).

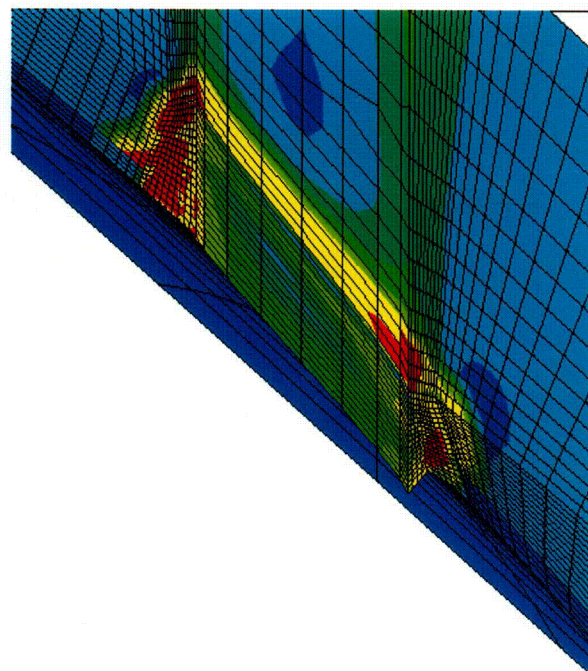
Technical Report to Support Relief Request ANO1-R&R-006

The stress contours for the residual stresses only and the steady state operating condition (residual + operating stresses) for the various repair cases evaluated are presented in Figures 4 through 7. In these figures, the left contour is for the “residual stress only” case and the right contour is from a case obtained from the steady state operating condition. The steady state operating condition is composed of the prevailing residual stress at the operating temperature and the stresses in the RVH due to pressure and temperature at steady state operating conditions. Hence, steady state operating conditions represent the prevailing stress state at the joint, which results from the combination of the component stress distributions.



ANO1CRDM(38.5d,48.5k,4/2.765,5.E-03,A) - Repair Only

Residual Stresses Only



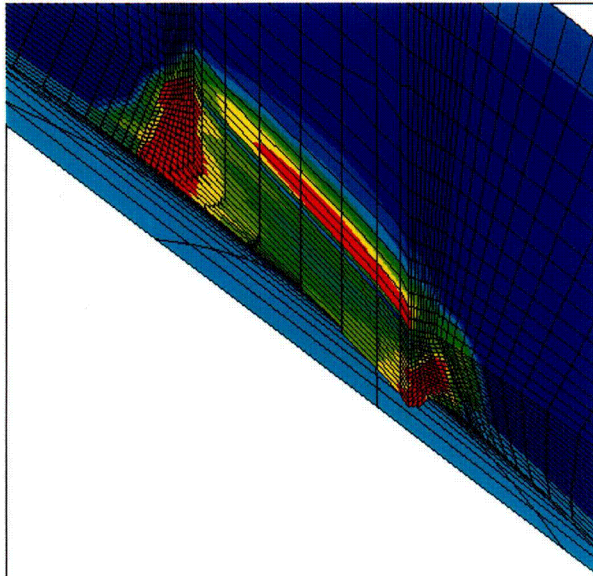
ANO1CRDM(38.5d,48.5k,4/2.765,5.E-03,A) - Repair + Operating

Residual + Operating (Steady State)

Figure 4: Stress contours for the “no chamfer case”. The zone of high residual stresses (red color) is observed to shrink in the steady state condition.

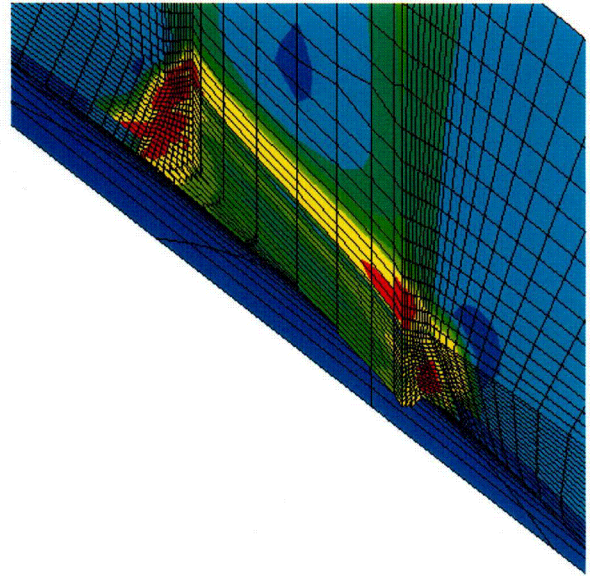
C04

Technical Report to Support Relief Request ANO1-R&R-006



ANO1CRDM(38.5d,48.5k,4/2.765,5.E-03,A) - Chamfer Only

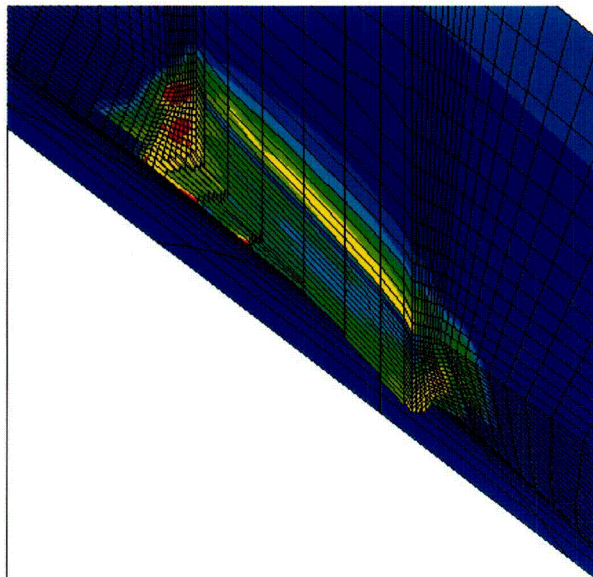
Residual Stresses Only



ANO1CRDM(38.5d,48.5k,4/2.765,5.E-03,A) - Chamfer + Operating

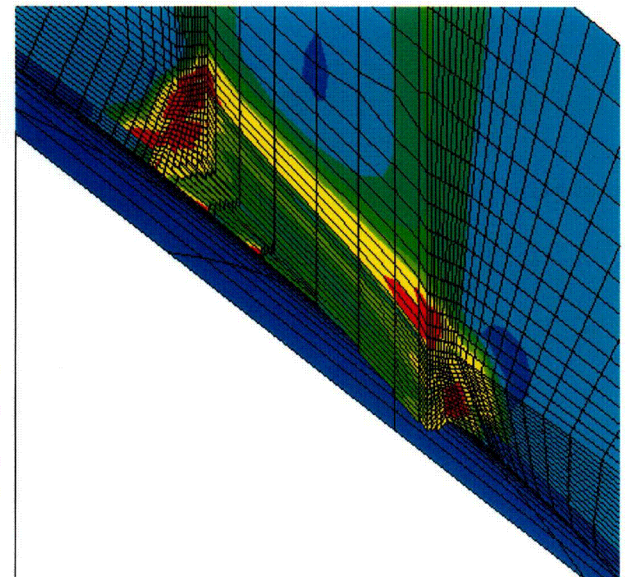
Residual + Operating (Steady State)

Figure 5: Stress contours for the “design minimum chamfer” case. The zone of high residual stresses (red color) is observed to shrink in the steady state condition.



ANO1CRDM(38.5d,48.5k,4/2.765,5.E-03,A) - Chamfer Only

Residual Stresses Only



ANO1CRDM(38.5d,48.5k,4/2.765,5.E-03,A) - Chamfer + Operating

Residual + Operating (Steady State)

Figure 6: Stress contours for the design “maximum chamfer” case. The zone of high residual stresses (red color) is observed to shrink in the steady state condition.

Technical Report to Support Relief Request ANO1-R&R-006

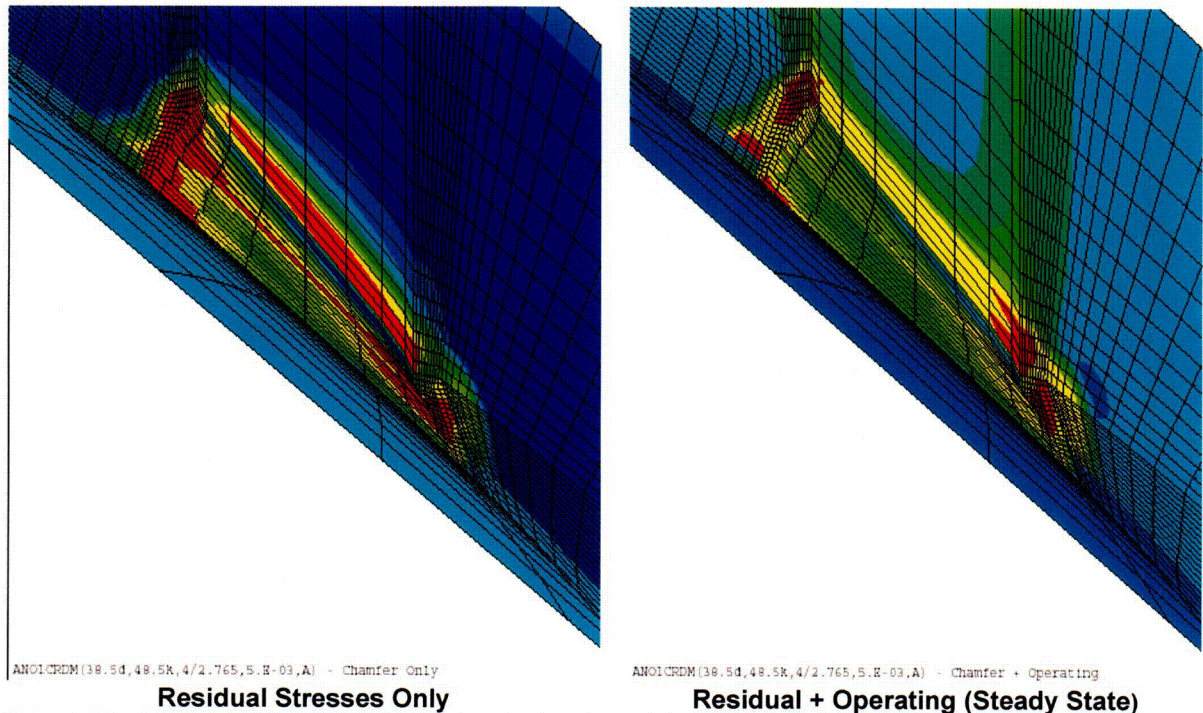
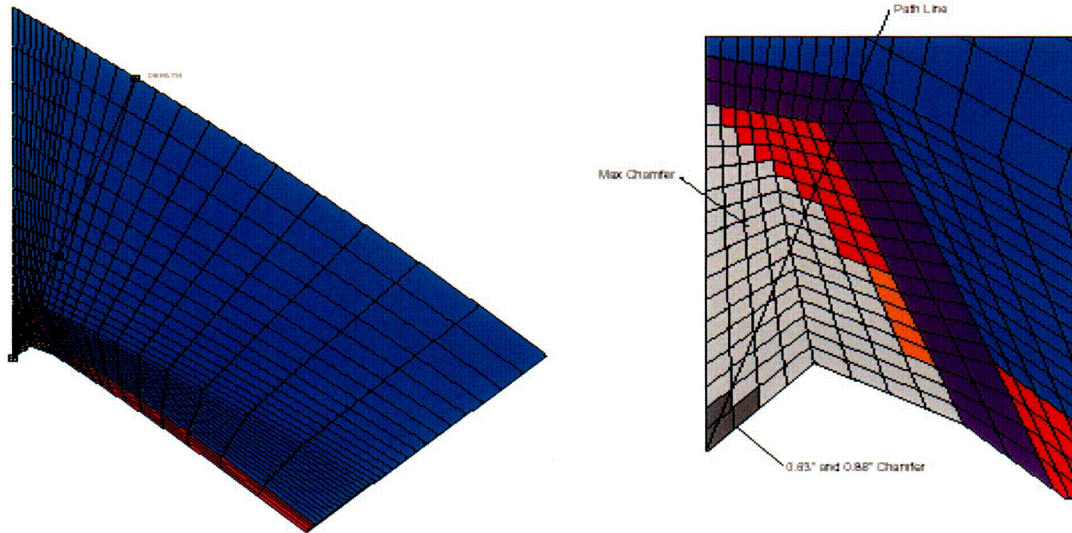


Figure 7: Stress contours for the “theoretical maximum chamfer” case. The zone of high residual stresses (red color) is observed to shrink in the steady state condition.

The hoop stress data obtained from the analysis for the various chamfer designs were evaluated along a path, which originates at the lower corner of the interface between the J-groove weld and the nozzle and extends towards the RVH outside diameter (OD) through the intersection point where the butter interface changes slope. This path is shown in Figure 8 for the downhill location and in Figure 9 for the uphill location. Also shown in these figures are the locations for the different chamfers considered in this analysis.

006

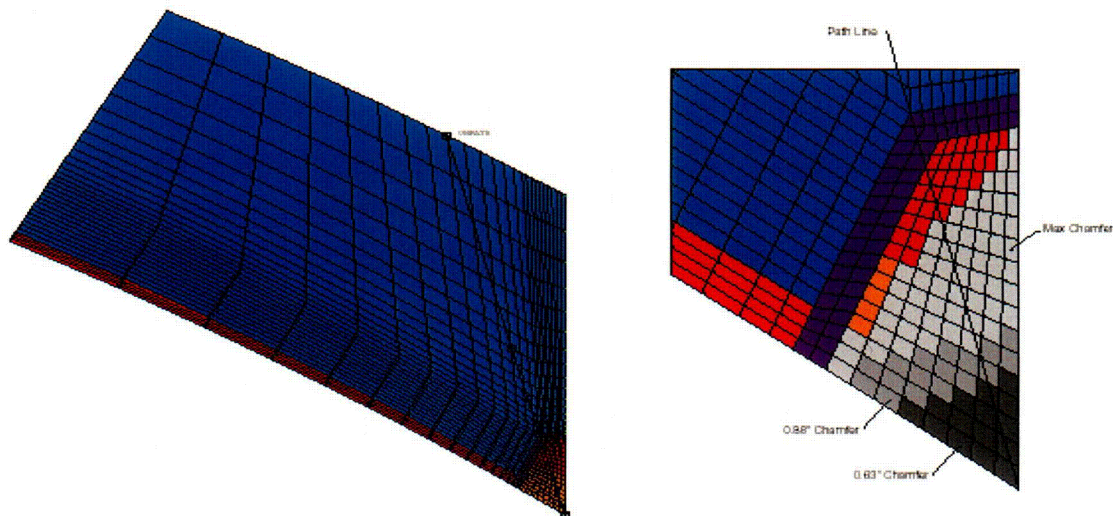
Technical Report to Support Relief Request ANO1-R&R-006



a) Path shown for full RVH

b) Path shown at J-groove weld

Figure 8: Path selected for hoop stress evaluation at the downhill location. The proposed chamfer designs and the path direction at the butter-RVH interface are shown in "b" (detail at J-groove weld).



a) Path shown for full RVH

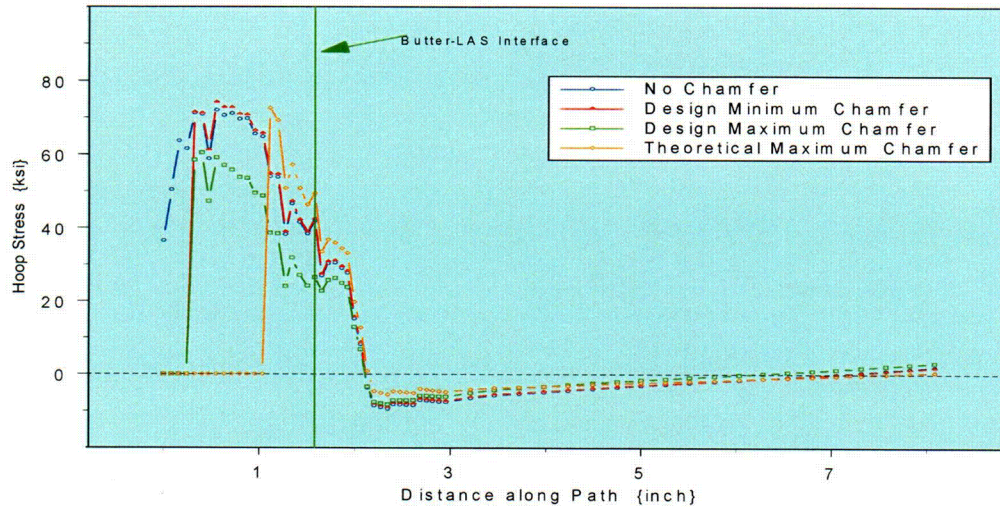
b) Path shown at J-groove weld

Figure 9: Path selected for hoop stress evaluation at the uphill location. The proposed chamfer designs and the path direction at the butter-RVH interface are shown in "b" (detail at J-groove weld).

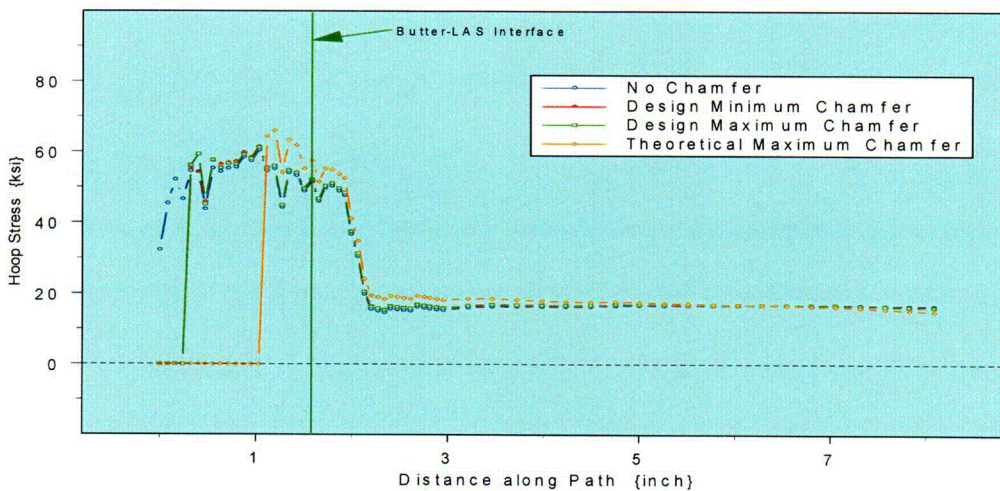
The hoop stress for the steady state and the "residual stress only" condition were extracted from the output files at about fifty locations. The hoop

Technical Report to Support Relief Request ANO1-R&R-006

stress distribution along this path for the various chamfer designs are presented in Figures 10 and 11.



a) Residual Stress Only

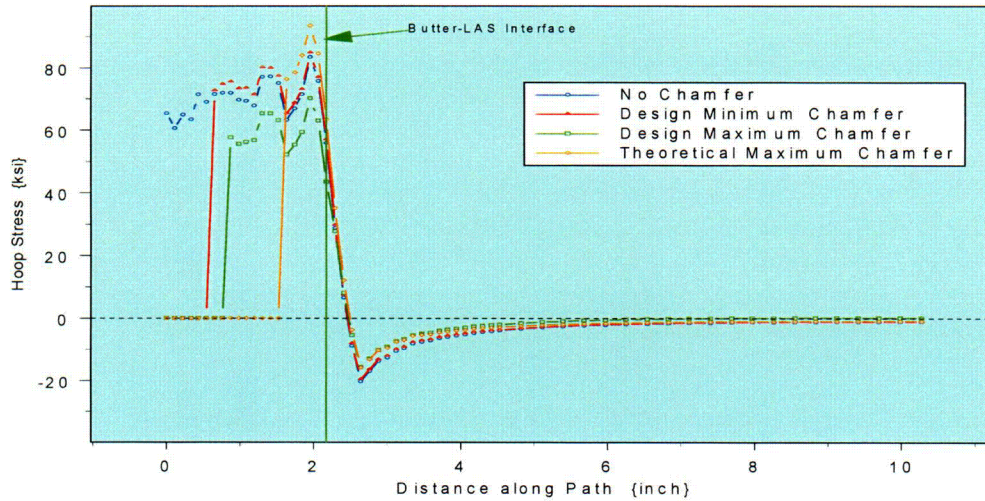


c) Steady State Condition

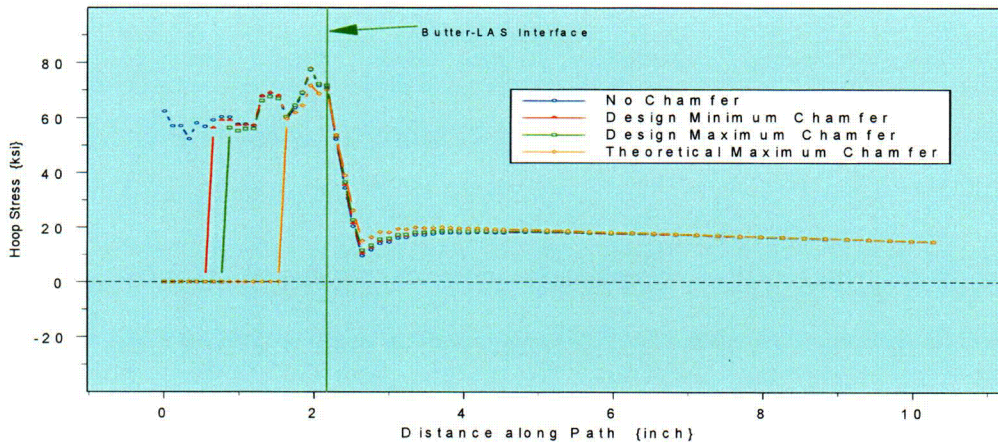
Figure 10: Hoop stress distribution at the downhill location along the selected path. The J-groove weld corner is at the left (0.0) and the RVH OD at the right (8.08"). The hoop stress is highly localized to the J-groove weld region. The effect of steady state operation is to soften the peak residual stress in the J-groove weld and eliminates the compression region immediately beyond the interface between the butter and the RVH. The effect of the chamfer design on the peak magnitude appears to be minimal. The location of the butter to RVH interface is shown by the green vertical line, which is located at 1.58 inches from the corner.

C08

Technical Report to Support Relief Request ANO1-R&R-006



a) Residual Stress Only



b) Steady State Condition

Figure 11: Hoop stress distribution at the uphill location along the selected path. The J-groove weld corner is at the left (0.0) and the RVH OD at the right (10.27"). The hoop stress is highly localized to the J-groove weld region. The effect of steady state operation is to soften the peak residual stress in the J-groove weld and eliminates the compression region immediately beyond the interface between the butter and the RVH. The effect of the chamfer design on the peak magnitude appears to be minimal. The location of the butter to RVH interface is shown by the green vertical line, which is located at 2.17 inches from the corner.

The stress contours shown in Figures 4 through 7 and the hoop stress plots along the selected path shown in Figures 10 and 11 show the following:

C09

Technical Report to Support Relief Request ANO1-R&R-006

- 1) The residual stress magnitude in the J-groove weld after the installation of various chamfer designs remains high.
- 2) There is some reduction of the total stress magnitude in the J-groove weld under steady state operating condition. This may be attributed to the bore hole dilation due to head expansion that occurs in this condition. However, it is important to note that the total stresses are dominated by the residual stress component.
- 3) The high hoop stresses are limited to the J-groove weld and to the vicinity of the buttering and the RVH base metal at the uphill and downhill locations. The remaining portion of the RVH has a much lower stress level.
- 4) The stress distributions at circumferential locations in between the uphill and downhill locations are much lower in magnitude (Figures 4 through 7). Hence the two locations for a bounding fracture mechanics analysis are the uphill and downhill locations.
- 5) Significant reduction in the stresses was not observed in the J-groove weld and its immediate vicinity for the various chamfer design simulations.

In order to assess the impact of residual stress on the total operating stress distribution, a comparison between the steady state conditions for the “design maximum chamfer” case from this evaluation was compared to the steady state operating stress obtained from Reference 1. In Reference 1 the steady state operating stress distribution does not include the residual stress component. This comparison is presented in Figure 12. In this figure, a third order polynomial fit to the stress data is also shown.

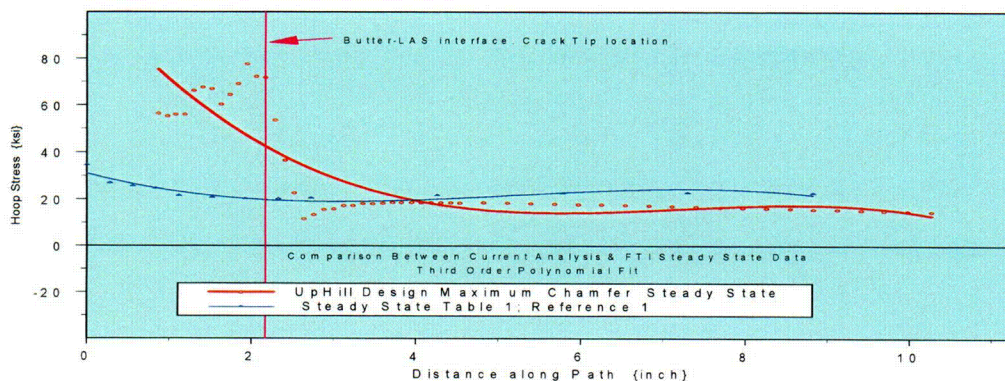


Figure 12: Comparison between current analysis and that from Reference 1 for steady state condition at the uphill location. The current analysis is dominated by residual stress that results in a higher stress magnitude in the J-groove weld. The third order polynomial does not adequately represent the stress distribution of the current analysis. Ignoring the residual stress contribution results in a much lower magnitude stress distribution in the J-groove weld region.

10

Technical Report to Support Relief Request ANO1-R&R-006

The following inferences can be made from Figure 12:

- 1) The third order polynomial does not adequately fit the data from the current analysis. Fracture mechanics analysis using closed form weight function methods, currently available, use a third order polynomial fit to describe the stress distribution; hence, using these formulations would introduce a significant error in the estimation of the SIF.
- 2) Fracture mechanics closed form solutions that use far field stresses necessitate linearizing the stress distribution. For the current application such a linearization would result in a high value for the membrane stress component, which would lead to an unrealistically high SIF.
- 3) Fracture mechanics analysis using closed form solutions cannot properly account for the highly localized stress distribution. Hence, the use of such solutions will not accurately characterize the prevailing SIF at the butter to RVH interface. The only rational alternative is to perform finite element-based fracture mechanics analysis.
- 4) The significant contribution of residual stress, in the region of interest, cannot be ignored. If the residual stress contribution to the SIF is not considered, the SIF would be severely underestimated. This aspect is explored further in the section titled "Discussion".

The numerical results from the stress analysis for the cases evaluated were transmitted electronically to the vendor performing the fracture mechanics analysis. The fracture mechanics analysis is discussed in the following section.

Technical Report to Support Relief Request ANO1-R&R-006

Linear Elastic Fracture Mechanics Analysis (LEFM)

Conceptual Basis

The LEFM analysis consisted of two separate steps:

- 1) Determine SIF along the crack front for the various imposed loads.
- 2) Perform a fatigue crack growth analysis.

For the determination of SIF, the finite element model developed for the residual stress analysis was modified to incorporate a fine mesh distribution in the region of interest (in the region where the crack was modeled). In the modified model the appropriate loading condition was simulated by a crack face pressure, which corresponded to the stress in the same region that was developed in an un-cracked structure upon imposition of the desired load. This method follows from the principle of superposition to determine the SIF, which can be described as follows [10]:

- 1) Sketch "a" shows the remote loading for an un-cracked plate; sketch "b" shows the same plate but with a central through-wall crack that is remotely loaded in tension and the crack is loaded in compression by a stress magnitude such that the crack is closed. These two loading conditions can be split as an algebraic sum of sketches "c" and "d" as depicted in Figure 13.
- 2) From the principle of superposition it can be shown that;

$$K_{\text{sketch "b"}} = K_{\text{sketch "c"}} + K_{\text{sketch "d"}} = 0 \text{ (un-cracked plate)}$$
 Therefore, $K_{\text{sketch "c"}} = -K_{\text{sketch "d}} = \sigma\sqrt{\pi a}$ (center cracked panel)
 Or, $K_{\text{sketch "d}} = \sigma\sqrt{\pi a}$
 When the crack face is pressurized by a pressure "p" which is equal and opposite of the remote stress "σ" then, $K_{\text{sketch "d}} = p\sqrt{\pi a}$.
- 3) The principle of superposition applies only to the region that is dominated by the stress singularity, which is in the immediate vicinity of the crack.

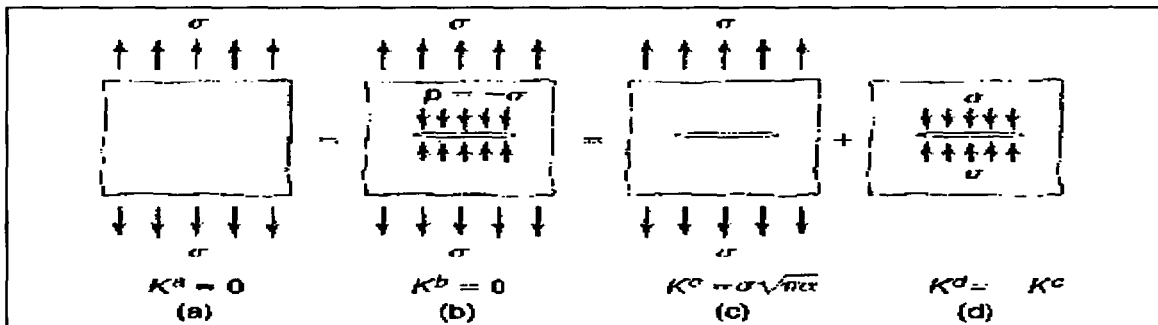


Figure 13: Determination of SIF for a pressurized center crack using the principle of superposition [10].

From the individual sketches the following can be defined [10]:

$$K^b = 0 = K^c + K^d; \text{ hence } K^c = -K^d;$$

Since $K^c = \sigma\sqrt{\pi a}$, and the crack face pressure is equal and opposite to the remote tension stress the SIF for sketch "c" becomes $K^c = p\sqrt{\pi a}$

Technical Report to Support Relief Request ANO1-R&R-006

The determination of SIF using finite element modeling method required special crack tip elements, which are located along the entire crack front. The crack tip elements were three-dimensional brick elements that had the mid-side nodes moved to the quarter point to simulate the proper singularity condition that exists at the crack tip.

Determination of Stress Intensity Factor

The assumed crack was modeled with a significantly refined mesh than that used in the stress analysis. A total of 50 nodes were used to define the crack front. Of these 50 nodes, 42 nodes represent crack between the low alloy steel and the buttering layer. The mid-side nodes of the crack front elements are moved to the quarter point location such that the singularity at the crack tip is maintained. Note that the first node is at the ID of the CRDM bore and the last fifty first node is at the RVH cladding wetted surface.

The chamfer design, which was shown in Figure 2, was modeled as follows:

- 1) The entire remnant J-weld including the butter weld was assumed to be cracked.
- 2) The flaw is modeled both on the uphill and downhill J-weld.
- 3) The hoop stresses obtained from the residual stress analysis, for an un-cracked geometry at the location of the remaining crack, was used to develop the crack face pressures for the radial-axial crack.
- 4) The internal pressure was modeled as crack face pressure and applied to the no chamfer case only. The resulting SIF for the internal pressure was added to the steady state SIF for the other cases. This approach is considered to be conservative, since, the SIF due to the internal pressure is maximized.
- 5) The intact regions are modeled with symmetry boundary conditions that represent material and geometric continuity.

The finite element model of the flaw geometry, including the loading applied to the crack face is shown in Figure 14 for the "no chamfer case". The SIF at all the crack tip locations were determined using the finite element post processing routine. The SIF at all locations, including those in the cladding were determined. Since a portion of the assumed crack is located at the J-groove weld to the stainless steel cladding interface (8 nodes from the cladding end), the SIF for these locations need not be considered for the evaluation of non-ductile failure. Therefore, the maximum SIF used in the evaluation with respect to the allowable fracture toughness prescribed in Reference 8 were from the nodes located on the low alloy steel interface with the buttering layer. The allowable SIF for the carbon steel was calculated based on upper shelf toughness, and the specification of IWB-3613(b) and IWB-3613(c) of Reference 8, are as follows:

Technical Report to Support Relief Request ANO1-R&R-006

Normal and Upset conditions {IWB-3613(b)}: 63.25 ksi√in.
Emergency and Faulted condition {IWB-3613(c)}: 141.44 ksi√in.

The LEFM analysis for the various cases considered was performed [11] as follows:

- 1) **No Chamfer:** The as-counterbored condition was analyzed for the steady state, residual stress only, and the internal pressure acting on the crack face. This represented a base case for comparison purposes and was used to obtain a conservative estimate of SIF due to crack face pressure. The specific case for the internal pressure acting on the crack face provides a maximum SIF because the force created by the internal pressure is a maximum for this case. The chamfer cases, which have a lower crack face area, the force due to the internal pressure acting on the crack face would be lower than that for the no chamfer case. The SIF obtained from this case was added to the steady state SIF for the other cases as needed.
- 2) **Design Minimum Chamfer:** Only steady state and residual stress only loadings were evaluated for this case. Transient operating stresses were evaluated for the maximum design chamfer case.
- 3) **Design Maximum Chamfer:** The SIF were calculated for the steady state, residual stress, and the four transient conditions considered in the stress analysis. A comparison of the results between the steady state and the transient conditions showed that the SIF for the transient condition were very close to that from the steady state condition, due to the predominant contribution of the residual stress component. Hence, it was not necessary to calculate the SIF for the transients for each of the chamfer conditions analyzed.
- 4) **Theoretical Maximum Chamfer:** Only steady state and residual stress conditions were analyzed. This geometry was analyzed to evaluate the effect of varying chamfer size on the resulting SIF.

No Chamfer Case

This geometry provides a base case for the comparison of the SIF as it relates to the chamfer size. This case also provided the opportunity to obtain a conservative upper bound for the SIF owing to the internal pressure acting on the crack face. The finite element model showing the application of crack face pressure based on the residual stress and steady state conditions are presented in Figure 14. The crack face pressure is simulated on the entire region that is assumed cracked (i.e. J-groove weld and buttering layer). The remaining region, which is not cracked, has no pressure application. The crack tip nodes are along

Technical Report to Support Relief Request ANO1-R&R-006

the crack front between the buttering and RVH interface (between the white arrows along the RVH boundary). In other cases (figures) the crack front is located along the boundary shown in Figure 14 and, hence, not shown in the other figures.

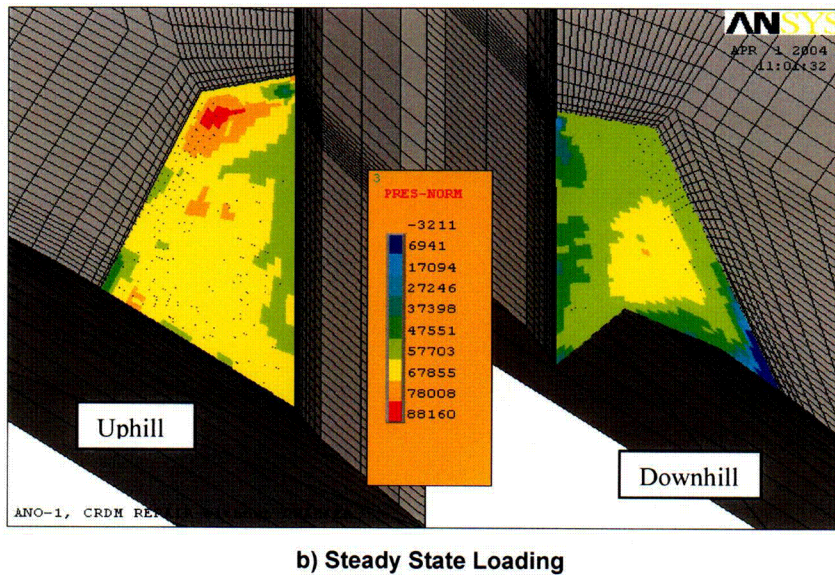
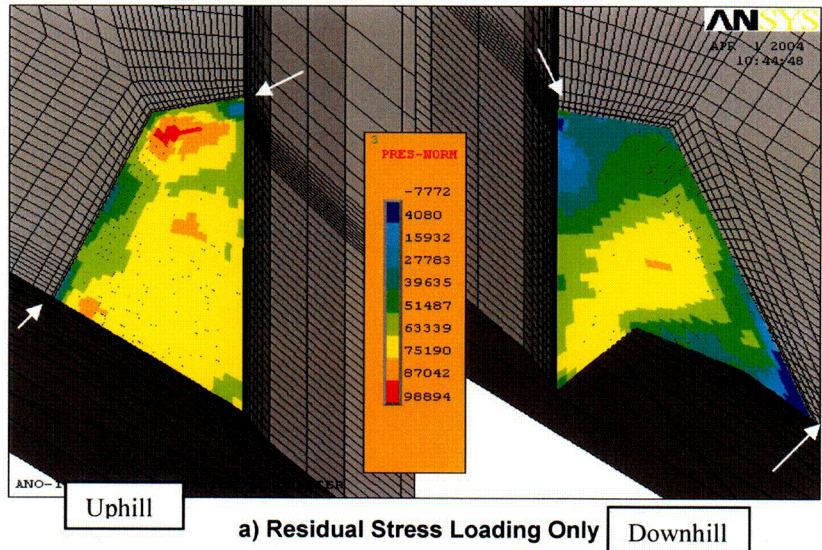


Figure 14: Finite element fracture mechanics model for the no chamfer case. The residual loading is shown in "a" and the steady state loading in "b". A small compressive zone on the downhill crack where it intersects the RVH cladding is observed.

CU

Technical Report to Support Relief Request ANO1-R&R-006

The steady state loading tends to make the stress distribution more uniform and increases the magnitude (color change). The SIFs for this case are shown in Figure 15.

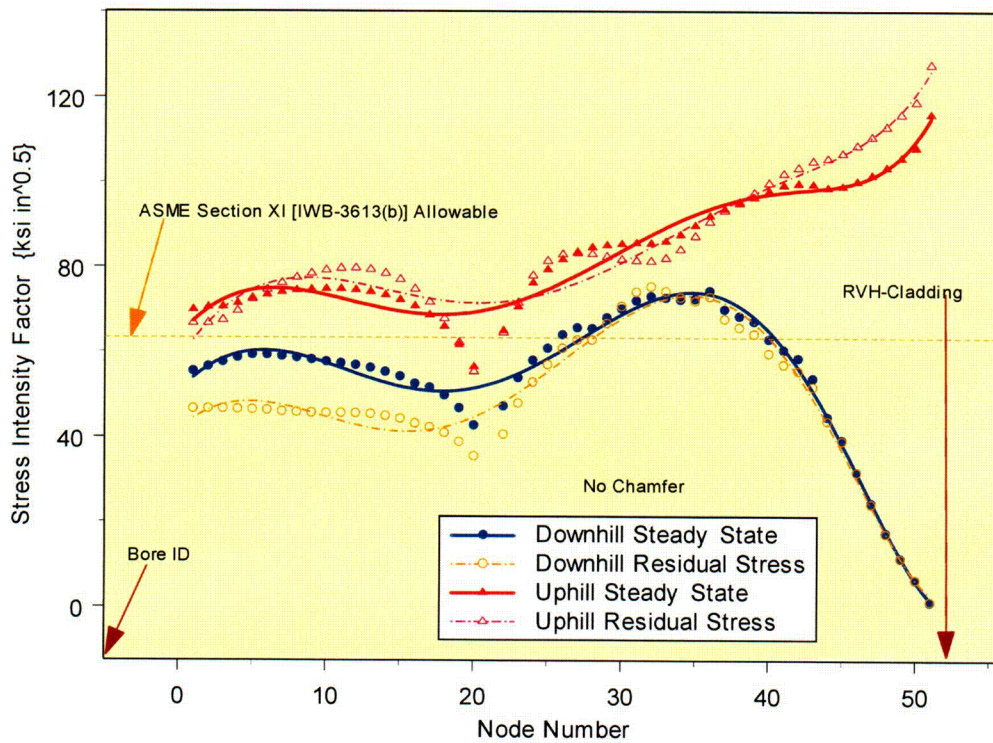


Figure 15: SIF plot for the no chamfer case. The SIF due to residual stress (open symbol) and steady state condition (closed symbol) for both the uphill and downhill cracks are shown. A sixth order polynomial fit to the data is also shown. Significant difference between the residual stress and steady state condition is not observed.

From Figure 15 the following observations are made:

- 1) The SIF for the uphill crack is higher than that for the downhill crack.
- 2) There is no significant difference between the SIF for the residual stress and steady state condition. This indicates that the residual stress distribution is the major contributor to the SIF.
- 3) The ASME Section XI allowable [8] is exceeded for certain locations along the crack front on the downhill side and for all locations on the uphill side.
- 4) The upper end of the crack, where the crack intersects the bore ID is on the left end of the graph. The right end of the graph is the location

Technical Report to Support Relief Request ANO1-R&R-006

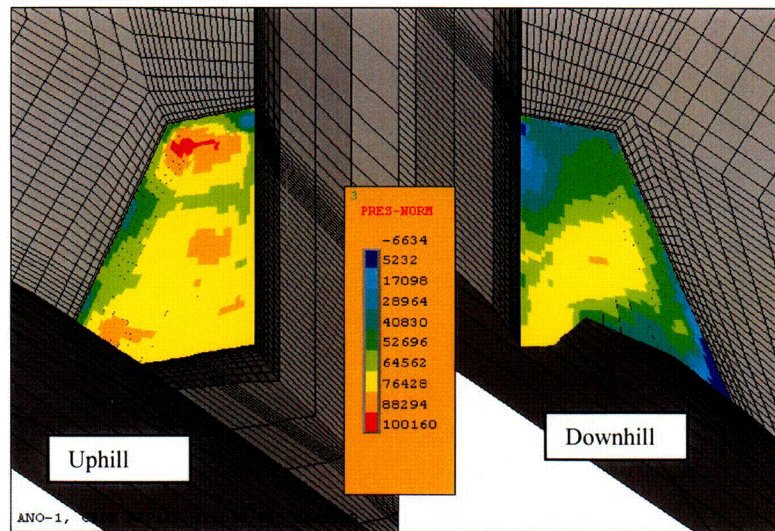
of the interface between the assumed flaw tip that is located between the buttering and the RVH-cladding on the wetted surface of the RVH. The node numbers representative of the crack front interface with the low alloy steel extends from node number 1 to node number 43.

- 5) A sixth order polynomial fit provides a reasonable approximation of the SIF distribution along the crack front. At the location of the transition of the J-weld prep knee, a sharp drop in the SIF data (individual points) occurs whereas the fitted line shows a smoother drop. The knee of the weld prep was approximated in the model and resulted in a sharp corner, which may be the reason for the sharp drop. However, the fitted line smoothes out the drop and may be more representative of the actual geometry.

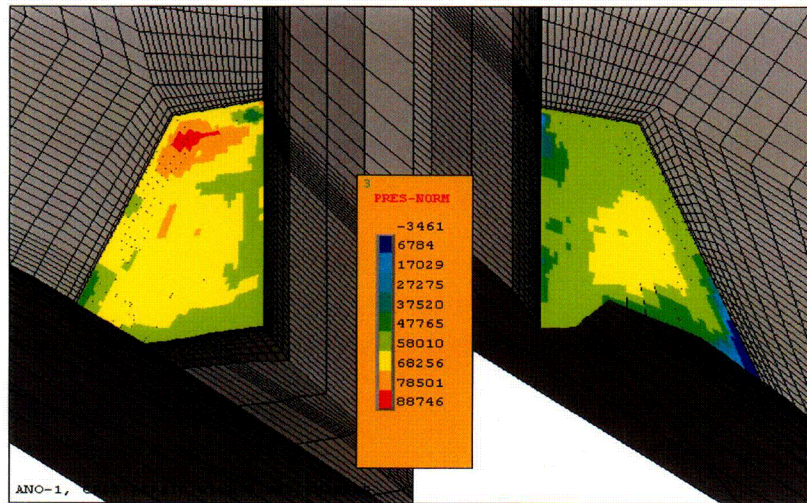
Design Minimum Chamfer Case

This case represents the chamfer that could be installed following the minimum dimensions provided in Reference 9. The crack face loadings for this case are shown in Figure 16. The chamfer on the uphill is visible but on the downhill the chamfer is very small and is barely noticeable in the figure.

Technical Report to Support Relief Request ANO1-R&R-006



a) residual Stress Loading Only



b) Steady State Loading

Figure 16: Finite element fracture mechanics model for the design minimum chamfer case. The residual loading is shown in "a" and the steady state loading in "b". A small compressive zone on the downhill crack where it intersects the RVH cladding is observed.

Figure 16 shows similar features to those in Figure 14. The SIF for the minimum design chamfer case are presented in Figure 17.

C13

Technical Report to Support Relief Request ANO1-R&R-006

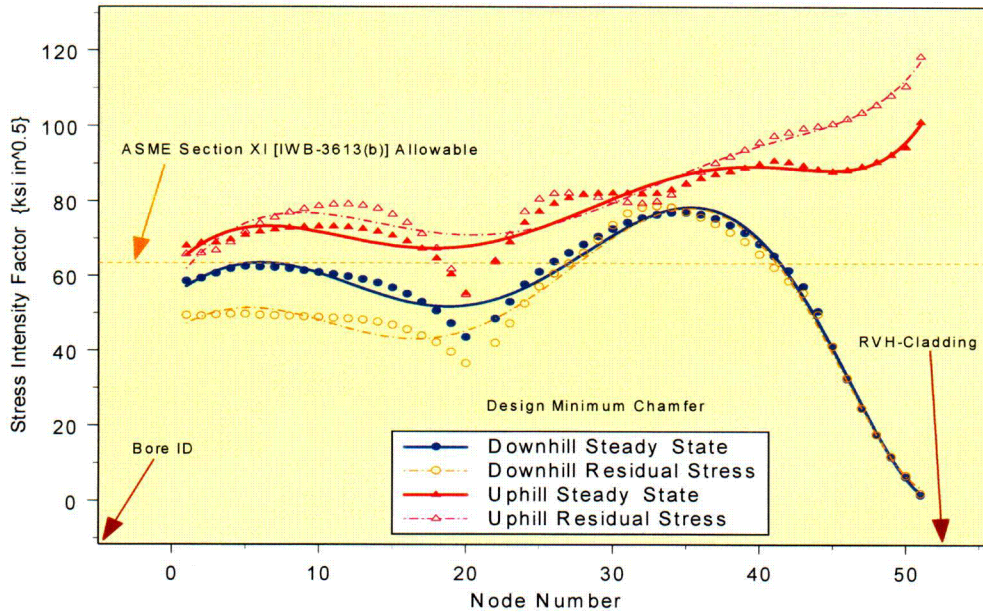


Figure 17: SIF plot for the design minimum chamfer case. The SIF due to residual stress (open symbol) and steady state condition (closed symbol) for both the uphill and downhill cracks are shown. A sixth order polynomial fit to the data is also shown. Significant difference between the residual stress and steady state condition is not observed.

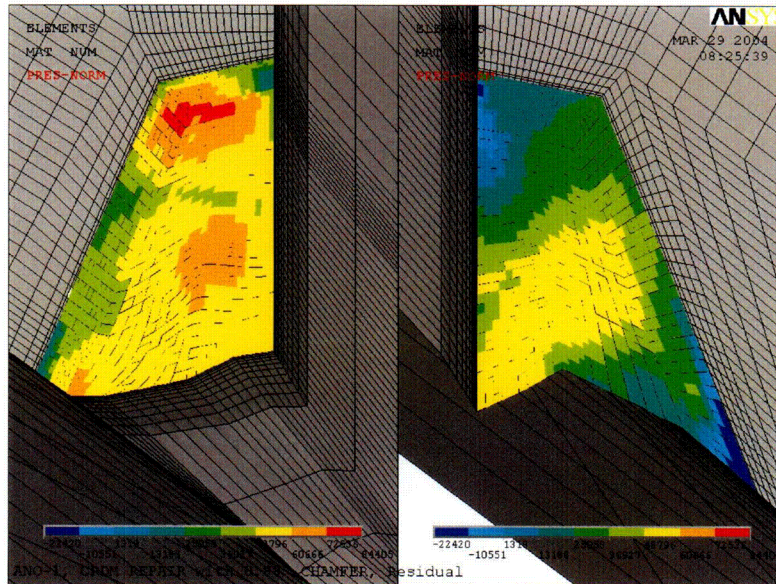
The node description for this case is similar to the information provided in item four (4) in the no chamfer case. The behavior of the SIF distribution in Figures 15 and 17 are very similar. Hence, the same observations, made from Figure 15 apply to Figure 17. The magnitude of the SIF is slightly different between the two figures. For the downhill crack there appears to be a slight increase and for the uphill crack a slight decrease when compared to Figure 15 (no chamfer case).

Design Maximum Chamfer Case

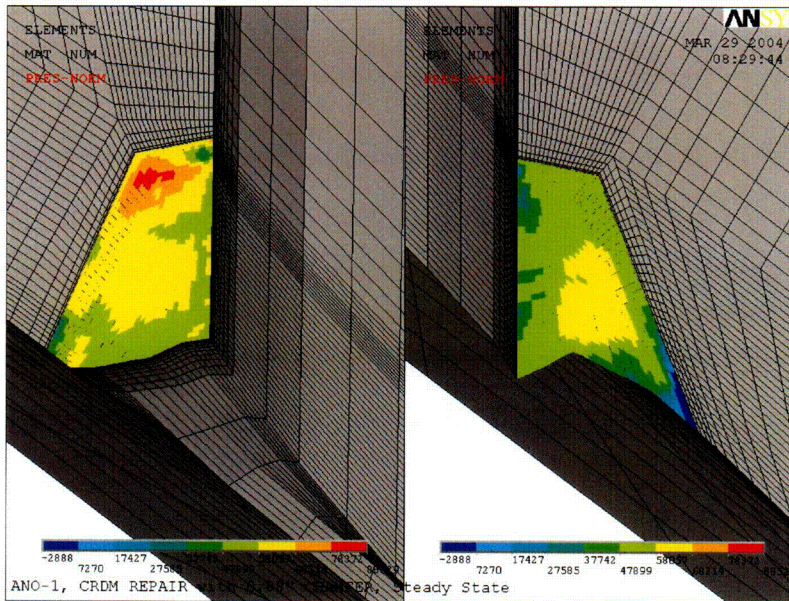
This case represents the chamfer that could be installed following the maximum dimensions provided in Reference 9. The crack face loadings for this case are shown in Figure 18. The chamfer on the uphill is visible, but on the downhill, the chamfer is small and is barely noticeable in the figure.

C14

Technical Report to Support Relief Request ANO1-R&R-006



a) Residual Stress Loading Only



b) Steady State Loading

Figure 18: Finite element fracture mechanics model for the design maximum chamfer case. The residual loading is shown in “a” and the steady state loading in “b”. A small compressive zone on the downhill crack where it intersects the RVH cladding is observed.

Figure 18 shows similar features to those in Figure 14. The SIF for the minimum design chamfer case are presented in Figure 19.

C15

Technical Report to Support Relief Request ANO1-R&R-006

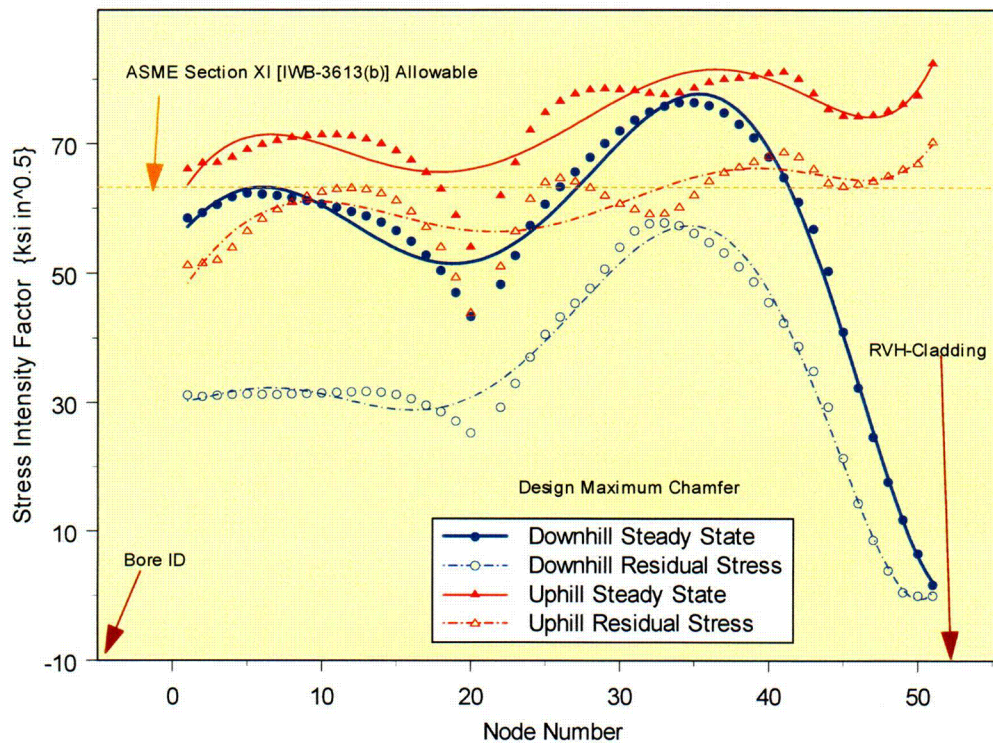


Figure 19: SIF plot for the design maximum chamfer case. The SIF due to residual stress (open symbol) and steady state condition (closed symbol) for both the uphill and downhill cracks are shown. A sixth order polynomial fit to the data is also shown. Though a difference between the residual stress and steady state condition is observed, the SIF at some crack locations exceed the ASME Section XI allowable.

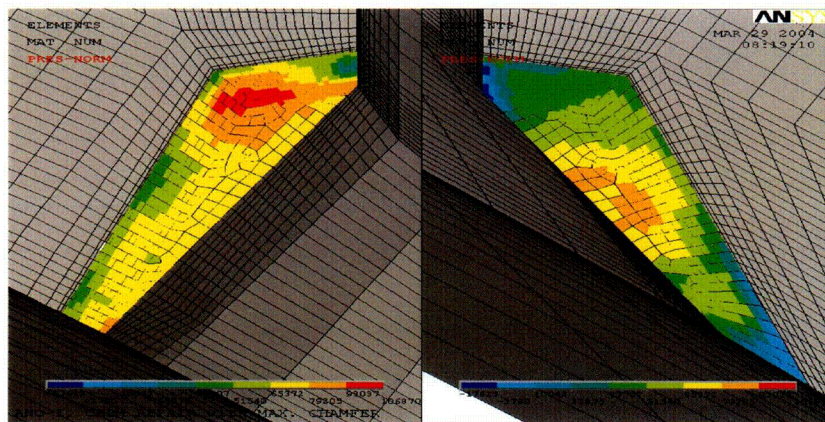
The node description for this case is similar to the information provided in item four (4) in the no chamfer case. The behavior of the SIF distribution in Figures 15 and 19 are similar. Hence, the same observations made from Figure 15 apply to Figure 19. The magnitude of the SIF is slightly different between the two figures. For the downhill crack there appears to be a slight increase and for the uphill crack a slight decrease when compared to Figure 15 (no chamfer case). Though there is a reduction in the SIF magnitude compared to the no chamfer case, the SIF at some crack front locations were found to exceed the allowable value of ASME Section XI IWB-3613(b) [8].

C16

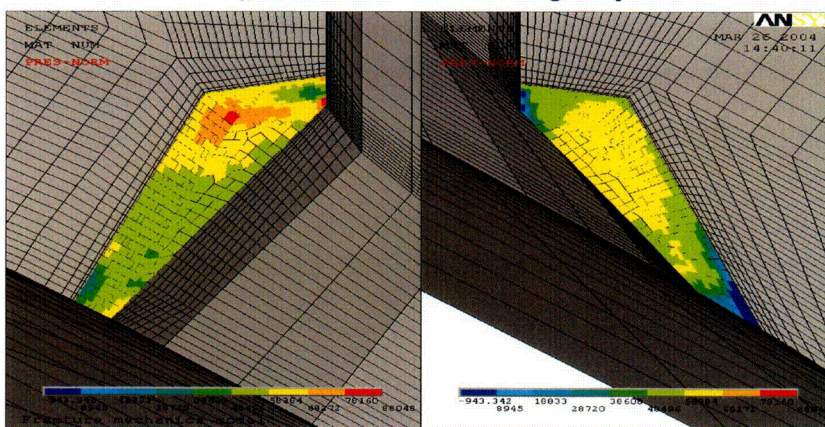
Technical Report to Support Relief Request ANO1-R&R-006

Theoretical Maximum Chamfer Case

This case was evaluated to ascertain the maximum theoretical benefit of installing a chamfer on the J-groove weld remnant. The model, as shown in Figure 2, removes a major portion of the J-groove weld remnant on the uphill side. The remnant on the downhill side is removed by following the contour along the periphery of the weld as rotated from the uphill towards the downhill side. However, this theoretical maximum chamfer cannot be installed in the field since it would require extensive tooling modification and testing. Therefore, the evaluation of this concept was to ascertain whether or not a theoretical maximum removal would enable satisfying the allowable limit of the ASME Section XI, IWB-3613(b) [8]. The finite element model for the SIF determination is shown in Figure 20.



a) Residual Stress Loading Only



b) Steady State Loading

Figure 20: Finite element fracture mechanics model for the theoretical maximum chamfer case. The residual loading is shown in "a" and the steady state loading in "b". A small compressive zone on the downhill crack where it intersects the RVH cladding is observed.

C17

Technical Report to Support Relief Request ANO1-R&R-006

Figure 20 shows similar features to those in Figure 14. The SIF for the minimum design chamfer case are presented in Figure 21.

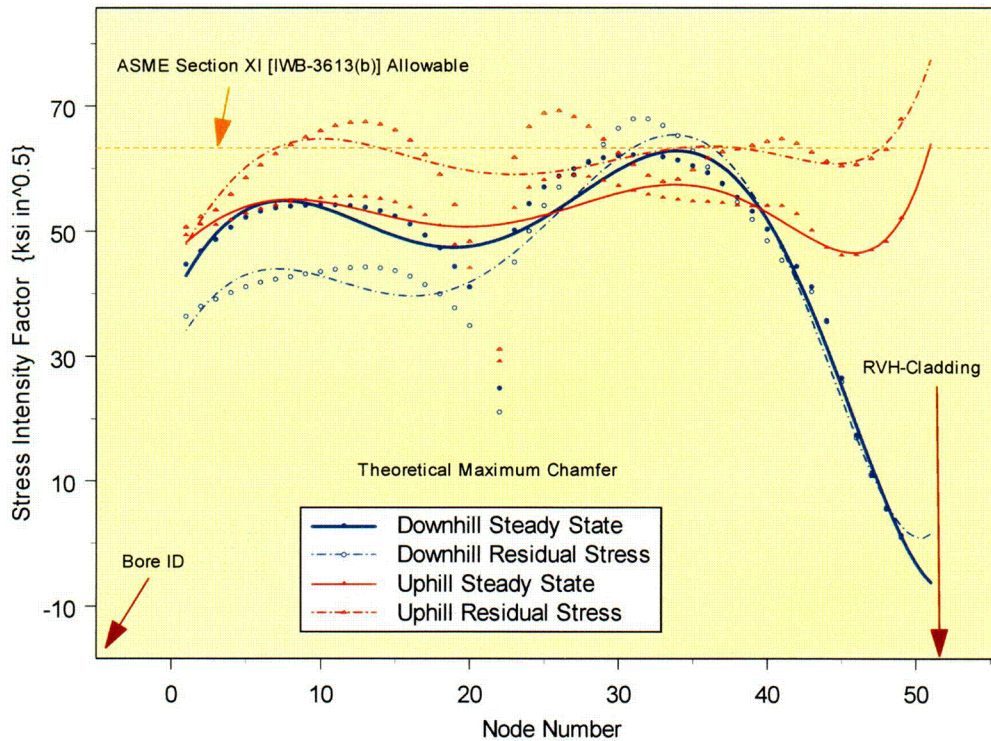


Figure 21: SIF plot for the theoretical maximum chamfer case. The SIF due to residual stress (open symbol) and steady state condition (closed symbol) for both the uphill and downhill cracks are shown. A sixth order polynomial fit to the data is also shown. Though a difference between the residual stress and steady state condition is observed, the SIF at the downhill crack location for the steady state condition exceeds the ASME Section XI allowable.

The node description for this case is similar to the information provided in item four (4) in the “no chamfer case”. The behavior of the SIF distribution in Figures 15 and 21 are similar. Hence, the same observations made from Figure 15 apply to Figure 21. The magnitude of the SIF is slightly different between the two figures. Though there is a reduction in the SIF magnitude compared to the no chamfer case, the SIF at some downhill crack front locations, for the steady state condition, were found to exceed the allowable value of ASME Section XI IWB-3613(b) [8].

Technical Report to Support Relief Request ANO1-R&R-006

Internal Pressure Applied to Crack Face

The application of the reactor coolant system (RCS) internal pressure was analyzed as a separate case using the “no chamfer model”. The no chamfer model has the highest crack face area; hence, the SIF resulting from the application of the internal pressure on the crack face will be maximized. The SIF obtained from this analysis was added to the respective steady state solutions from the three chamfer cases. In Figure 22 for the “no chamfer case”, the effect of applying the RCS internal pressure on the crack face is shown. The SIF from the steady state analysis is presented for comparison. The impact of considering the RCS pressure on the crack face is evident as it shows a noticeable increase in the SIF.

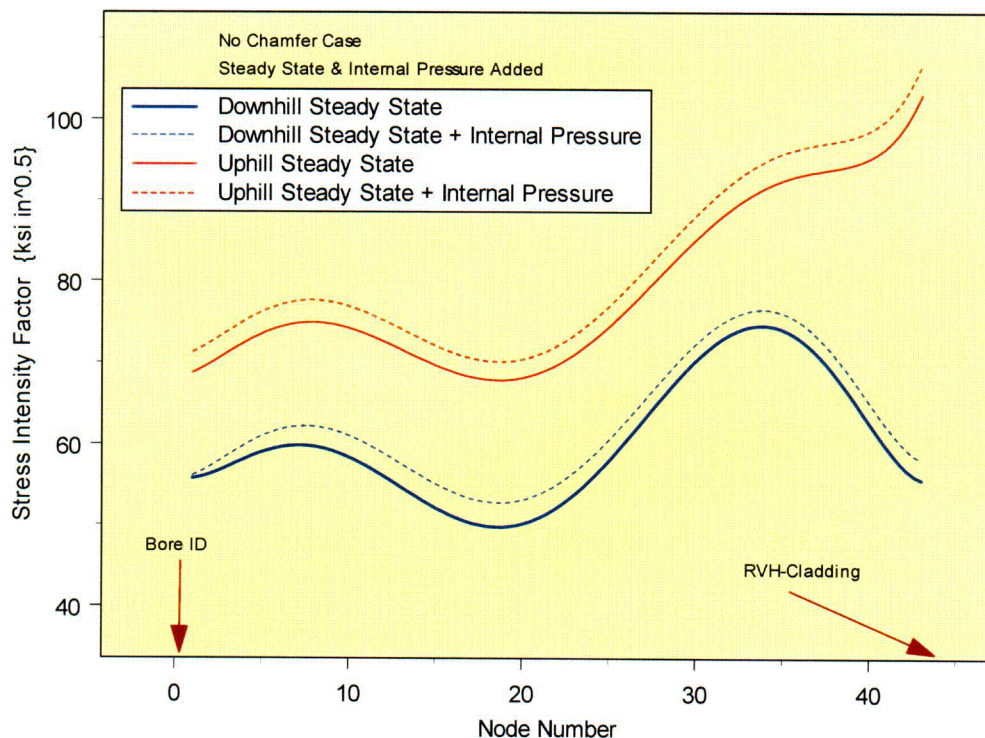


Figure 22: Effect of RCS pressure on no chamfer case. The RCS pressure when added to the crack face results in an increase in the SIF. The solid lines are for the total SIF (Residual + Operating + RCS pressure on Crack face) and the broken lines for the steady state case (Residual + Operating).

The SIF obtained for the RCS pressure on the crack face from the analysis of the no chamfer case was added to the steady state (residual + operating) results for the three chamfer cases. In Figures 23 and 24, the results

Technical Report to Support Relief Request ANO1-R&R-006

for the total SIF (Residual + Operating + RCS pressure on crack face) for the three chamfer cases are presented and compared to the ASME Section XI, IWB-3613(b) [8] allowable value. Figure 23 presents the result for the crack centered

at the downhill location and Figure 24 for the crack centered at the uphill location. From these two figures it is observed that the ASME Section XI allowable is exceeded either for both crack locations (design chamfer) or at the downhill location for the theoretical maximum chamfer. This result shows that chamfering to reduce the J-weld remnant size does not result in an acceptable SIF.

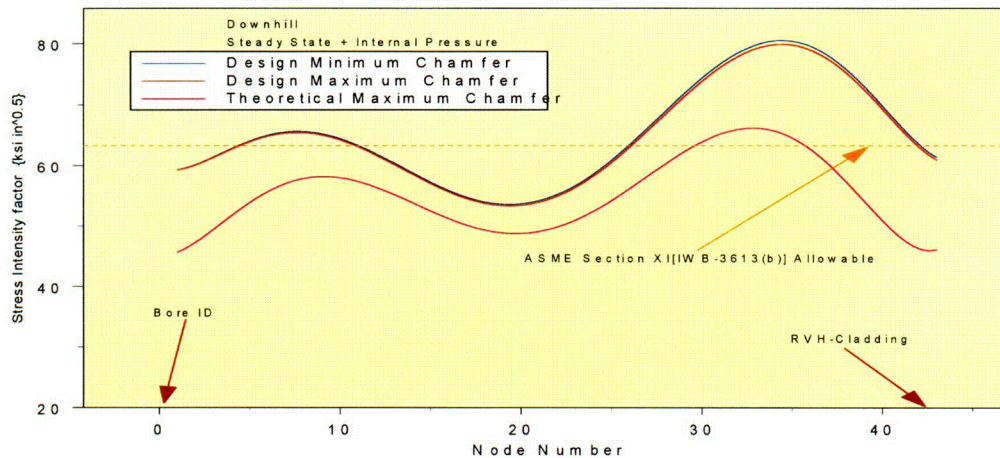


Figure 23: Comparison of total SIF for the three chamfer cases at the downhill location. There appears little difference between the two design chamfer cases (minimum and maximum); because the size of the chamfer at the downhill location for both cases were very small when compared to the uphill side. The SIF for the theoretical maximum chamfer is also found to exceed the ASME Section XI allowable.

C20

Technical Report to Support Relief Request ANO1-R&R-006

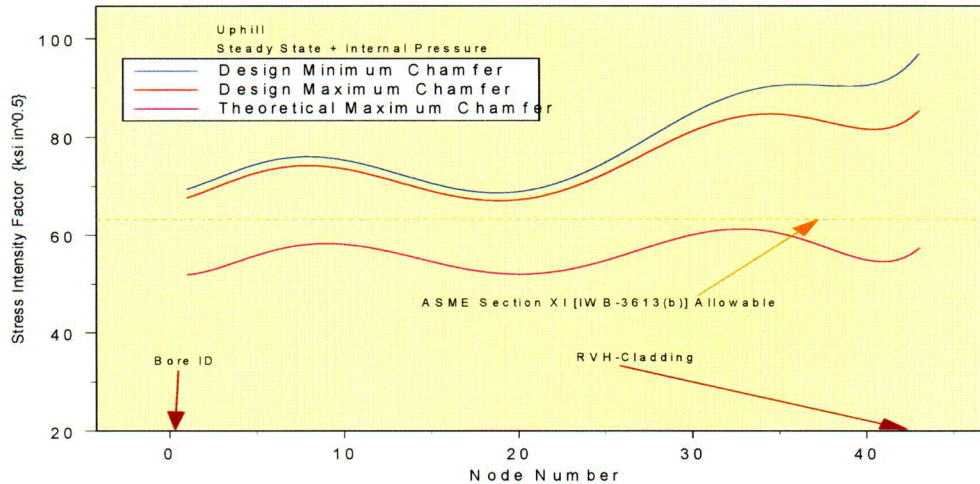


Figure 24: Comparison of total SIF for the three chamfer cases at the uphill location. A reduction in the SIF from the design minimum to theoretical maximum chamfer is observed. Neither of the design chamfers meets the ASME Section XI allowable.

The fracture mechanics analysis method, presented above, conforms to the NRC expectation of Reference 13. The results for the maximum SIF along the crack front interface with the low alloy steel RVH obtained from Reference 11, is presented in Table 1. The SIF values that were above the ASME Section XI allowable [8] are shown in red font.

Table 1 : Maximum SIF from LEFM Analysis

J-groove Weld Remnant Configuration	Maximum Applied Stress Intensity Factor ¹ (ksi√in)		
	Steady State Operation ²	Residual Stresses Only ³	Operating Condition Only ⁴
No Chamfer	77.4 – Downhill 103.4 - Uphill	75.3 – Downhill 115.70 – Uphill	2.1-Downhill Note 5 – Uphill
Design Minimum Chamfer	80.0 –Downhill 94.4 - Uphill	76.99 – Downhill 90.70 – Uphill	3.01 – Downhill 3.7 – Uphill
Design Maximum Chamfer	79.4 – Downhill 84.8 - Uphill	76.38 – Downhill 81.10 – Uphill	3.02 – Downhill 3.7 Uphill
Theoretical Maximum Chamfer	65.2 – Downhill 62.5 - Uphill	62.19 – Downhill 58.85 – Uphill	3.01 –Downhill 3.65 - Uphill

Notes:

- 1) The applied SIF is based on considering the three conditions provided in 2, 3, and 4 below.
- 2) The steady state condition is the combined SIF based on residual stress plus steady state operating stresses (pressure and temperature).
- 3) The residual stress condition is based on the residual stress state after completion of the chamfer on the J-groove weld as indicated by the configuration column.
- 4) The operating condition is the difference between the steady state condition and the residual stress state. This column provides the SIF estimate due to the operating condition alone.
- 5) The SIF due to the residual stress is higher than at steady state operating condition.

C21

Technical Report to Support Relief Request ANO1-R&R-006

The results presented in Table 1 show that for most of the cases evaluated the maximum SIF exceeds the ASME Section XI allowable [8] value of $63.2 \text{ ksi}\sqrt{\text{in}}$.

Analysis of Transients

The transient analysis was performed on the design maximum chamfer geometry, because the fracture mechanics analysis results showed that there were very small differences in the SIF between the two chamfer designs (minimum and maximum). The transients considered, which were based on References 1 and 12, were as follows:

- 1) Heat-up {Normal & Upset condition}.
- 2) Cooldown {Normal & Upset condition}.
- 3) Reactor Trip {Normal & Upset condition}.
- 4) Inadvertent Rod Withdrawal {Accident/Faulted condition}.

The SIF results from the transient analysis are compared with the corresponding steady state SIFs, which are presented in Figure 25 for the downhill location and Figure 26 for the uphill location.

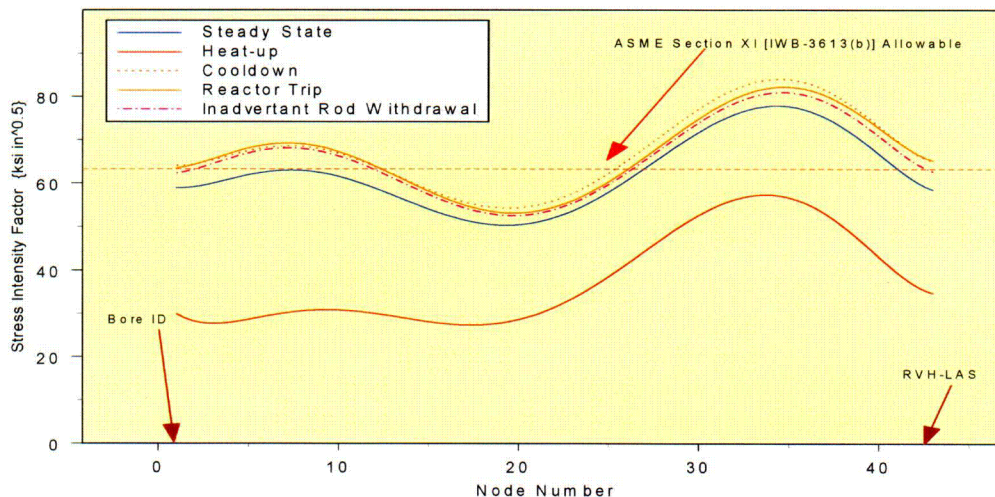


Figure 25: Results for transient analysis for the design maximum chamfer case at the downhill location. The cooldown, reactor trip, and the rod withdrawal transient SIF are slightly higher than that for the steady state condition. The distribution of the SIFs is very similar.

C22

Technical Report to Support Relief Request ANO1-R&R-006

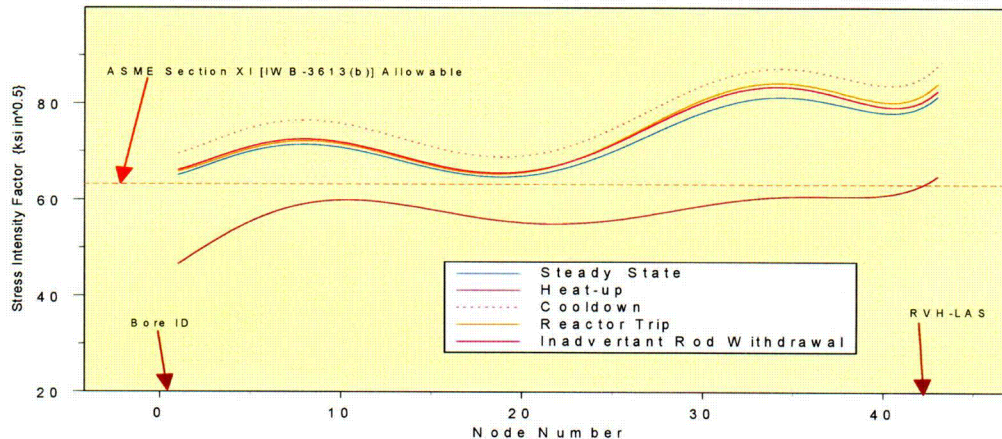


Figure 26: Results for transient analysis for the design maximum chamfer case at the uphill location. The cooldown, reactor trip, and the rod withdrawal transient SIF are slightly higher than that for the steady state condition. The distribution of the SIFs is very similar.

The results from the transient analysis, presented in Figures 25 and 26, indicate that the SIF during some of the transients are slightly higher than the steady state condition. The SIF for the two transients representing the normal and upset condition (Heat-up/cooldown and reactor trip) are the transients that would impose a fatigue loading at the crack tip. These transient results will be used to perform the fatigue crack growth analysis. The uphill location SIFs are higher than those at the downhill location. For the two transients that represent the normal and upset condition, the SIF are found to exceed the ASME Section XI allowable [8] for that condition. The inadvertent rod withdrawal is an accident condition and the resulting SIF is within the ASME Section XI allowable for accident condition [8].

Fatigue Crack Growth Analysis

The fatigue crack growth was computed from the transient analysis results described above. The fatigue crack growth was performed for one cycle of operation. The number of transient events was obtained from References 1 and 21. The transients considered for the fatigue crack growth were as follows:

- 1) Normal Heat-up/Cooldown - 6 cycles/year
- 2) Reactor Trip/Heat-up - 9 cycles/year

The fatigue crack growth law for light water environment presented in Appendix "A" in ASME Code, Section XI [8], was used for this evaluation. From the transient data presented for the uphill crack the maximum " ΔK " was found to be as follows:

Technical Report to Support Relief Request ANO1-R&R-006

- 1) Normal Heat-up/Cooldown - 38.7 ksi/in.
- 2) Reactor Trip/Heat-up - 39.2 ksi/in.

The constants for the fatigue crack growth equation were based on " ΔK " and the "R" ratio (K_{\max}/K_{\min}) which was 0.43. Based on these values the material constant " n " and the scaling constant " C_0 " were as follows:

- 1) Material constant " n " = 1.95 (Paragraph A-4300 of Reference 8)
- 2) Scaling constant " C_0 " = 1.179×10^{-7} (Paragraph A-4300 of Reference 8)

The fatigue crack growth for two cycles of operation showed the growth to be 0.005 inch. The extent of fatigue crack growth is very small and would not impact the SIF significantly. Therefore, the need to determine the end-of-operating cycle based SIF would not be necessary.

Technical Report to Support Relief Request ANO1-R&R-006

Elastic Plastic Fracture Mechanics Analysis (EPFM)

The results presented in Table 1 show that the acceptance criterion of IWB-3613(b) [8] are not met. In order to assess the true margin an EPFM analysis was performed. The EPFM analysis was performed for the "Design Minimum Chamfer" case since this configuration was the repair for the previous repairs and for repairs that may be required for the current refueling outage. The EPFM evaluation is documented in Reference 12 and presented in Appendix "A" of this report. Presented below is a summary of the analysis method and the results obtained from the analysis.

In the EPFM methodology the following steps are necessary:

- 1) The determination of the applicability of the EPFM method.
- 2) The material toughness expressed as the "J" integral as a function of crack size (a).
- 3) The "J" integral for the postulated crack size based on the applied loads.

Determination of Applicability:

In order to apply the EPFM methods it is necessary to ensure that the specific screening criterion is not violated. The screening criterion is obtained from Appendix "H" of Reference 8. Though this appendix was developed for ferritic piping the screening criteria is based on the failure analysis diagram (FAD) concept, and hence is applicable for the current work. The screening criterion is defined as:

$$SC = \frac{K_r}{S_r} \quad \text{for EPFM validity } 1.8 > SC > 0.2$$

Where:

$$K_r = \frac{K_{total}}{K_{Ic}} \quad \text{and} \quad S_r = \frac{\sigma_{peak}}{\sigma_{flow}}$$

K_{total} is the total SIF obtained from the LFM analysis presented earlier, and for the case considered the value from table 1 is 94.4 ksi√in.

K_{Ic} is the material fracture toughness, which in accordance with Appendix "A" of Reference 8 is 200 ksi√in.

σ_{peak} is the peak stress in the J-groove weld obtained from the finite element analysis described earlier and was determined from Reference 4 to be 88.5 ksi.

Technical Report to Support Relief Request ANO1-R&R-006

σ_{flow} is the material flow stress, which is defined as the average of the ultimate tensile strength and the yield strength, is obtained from ASME Section XI Part D. The value for the flow stress at operating temperature is 80.0 ksi. Substituting the values above into the equation for the screening criterion (SC) gives 0.43, which is clearly in the range defined for EPFM (shown above). Hence EPFM analysis is valid for the analysis of the J-weld remnant crack.

Determination of Material Toughness Curve

The determination of material toughness curves follows the guidance from Appendix "K" of Reference 8. Once again the guidance is for material toughness and is not component geometry specific. Hence, the approaches presented in Appendix "K" [8] are applicable to the current work. The three methods for determining the material toughness are:

- 1) A J-R (J is the J-integral and R the material resistance) curve may be generated by actual testing of the material following accepted test procedures; or
- 2) May be generated from a J-integral database obtained from the same class of material with the same orientation; or
- 3) An indirect method of estimating the J-R curve may be used, provided the method is justified for the material.

In this analysis method 3 was used and was based on Charpy "V-notch" correlation of Reference 14. The Charpy absorbed energy for the ANO-1 RVH was obtained at a single temperature (+10 °F) and the data is documented in the ANO-1 UFSAR, Table 4-16. Since the RVH was procured before the Summer of 1972 addenda to the ASME Code the Charpy testing was performed only on longitudinally oriented specimens. The Summer 1972 Addenda to the ASME Code, Section III, and subsection NB-2300 changed the Charpy testing requirements for Class I components. In these addenda the transverse orientation was prescribed for the testing. However, Reference 15 provides a method in paragraph B-1.1-3(a) to convert the longitudinal data to represent the data had the testing been done in the transverse orientation. The conversion is a reduction in the absorbed energy value obtained from longitudinal testing to 65% of the value. Since the material toughness curve required for the EPFM analysis is the Charpy upper shelf energy (USE) level it is necessary to estimate the USE based on the single temperature data. Additionally following the philosophy for the J-integral (item 2 above) that could be obtained from the same class of material with the same orientation, the USE for the ANO-1 RVH was estimated in the following manner:

- 1) The RVH material for ANO-1 is specified as ASME SA533 Gr. B-C11. The material that was tested to obtain the full curve

Technical Report to Support Relief Request ANO1-R&R-006

Charpy data was for Grand Gulf Nuclear Station (GGNS) which was also made to a similar specification (SA533 Gr. B-C11) and by the same manufacturer. These plates are from the reactor vessel beltline and hence the full transition curve data was obtained. In addition the plate thickness for the GGNS plates were 5.69 inches thick, which is close the ANO-1 RVH plate thickness of 6.6 inches. There is a paucity of full transition curve Charpy data because such data exists only for the beltline materials. In addition the PWR beltline material is considerably thicker. Therefore the use of the GGNS data for estimating the USE is justified.

- 2) The full transition curve data for the GGNS plates were obtained from Charpy testing conducted in the transverse orientation since these plates were procured to the winter 1972 Addenda. The certified material test reports that contain the Charpy data are provided in Appendix "B" of this report.
- 3) The single temperature data for the ANO-1 RVH, which was obtained from the ANO-1 UFSAR Table 4-16 was as follows:

Closure Head Flange: 62, 60 & 86 ft-lb;

Average = 69.33 ft-lb;

Corrected = 45.06 ft-lb MTEB 5-5, B-1.1-3(a)

Closure Head Center Disc: 62, 53 & 64 ft-lb;

Average = 59.67 ft-lb;

Corrected = 38.78 ft-lb MTEB 5-2, B-1.1-3(a)

Head Transition Piece: 61, 95 & 66 ft-lb;

Average = 74.00 ft-lb;

Corrected = 48.10 ft-lb; MTEB 5-2, B-1.1-3(a)

The corrected values, which represent the expected absorbed energy for a transverse oriented test, were used for the comparison and the estimation of the minimum USE for the ANO-1 RVH material.

- 4) The Data was plotted and fit with a fourth order polynomial. The 99% confidence bound for the fitted curve was also obtained. The reduced transverse data for ANO-1 RVH was plotted on the same graph as that for the GGNS material. The lowest USE for the GGNS materials was 94 ft-lbs. However, the Charpy testing data was limited to +212°F with a fracture appearance of 1% shear. Clearly the USE would have been higher had the testing continued to higher temperatures. The results of this data evaluation are shown in Figure 27.

Technical Report to Support Relief Request ANO1-R&R-006

- 5) The ANO-1 data is bounded by the lower 99% confidence line at + 10 °F and the USE that was to be used in the EPFM analysis is much lower than the USE for the lower 99% confidence line (Lowest USE = 94 ft-lb; Lower 99% confidence line USE = 98 ft-lb). Therefore the use of the minimum USE for the EPFM analysis of 94 ft-lb is justified, and is believed to conservatively represent the ANO-1 RVH materials, since the ANO-1 data is bounded by the 99% lower confidence bound.

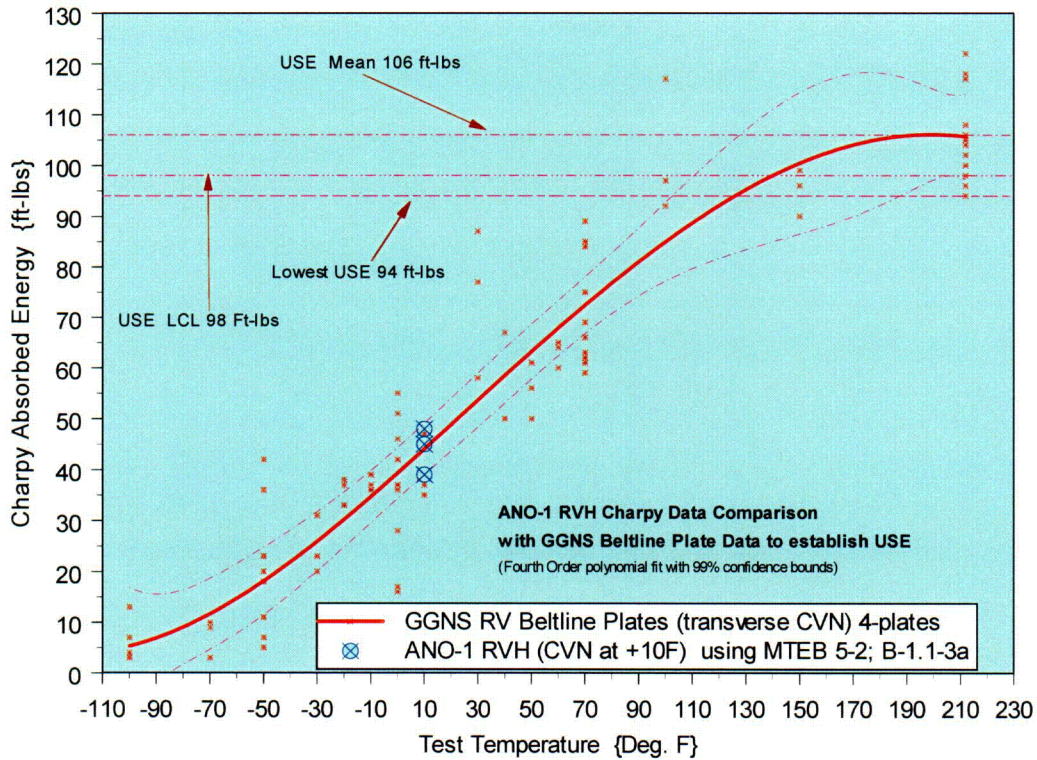


Figure 27: Charpy absorbed energy data. Transverse data from GGNS reactor vessel beltline plates. Also shown are the three ANO-1 RVH material data points after MTEB 5-2 conversion. The ANO-1 data is bounded by the GGNS data.

The Charpy USE can then be used, following the guidance of Reference 14, to determine the material toughness. The material toughness is defined [14] By a power law as:

$$J = C * (\Delta a)^m$$

C24

Technical Report to Support Relief Request ANO1-R&R-006

Where:

- J = J-integral
- C = Constant. (correlation coefficient)
- Δa = Crack extension
- m = Constant. (correlation exponent)

Reference 14 provides the method to obtain the constants, based on Charpy USE, as follows:

- 1) To demonstrate the applicability of the method in Reference 14, the Charpy USE used for the current analysis is plotted on the J-integral vs. Tearing Modulus (J-T) graph of Reference 14, and is presented in Figure 28. The data in the graph was obtained from several reactor vessel steels both in the un-irradiated and irradiated conditions. This data represents a spread in the USE values. The lowest USE value and the ANO-1 Charpy absorbed energy value of 40 ft-lb (MTEB 5-2 converted) are shown in Figure 28. The data used in the current analysis is shown to be properly represented by the curves from Reference 14.

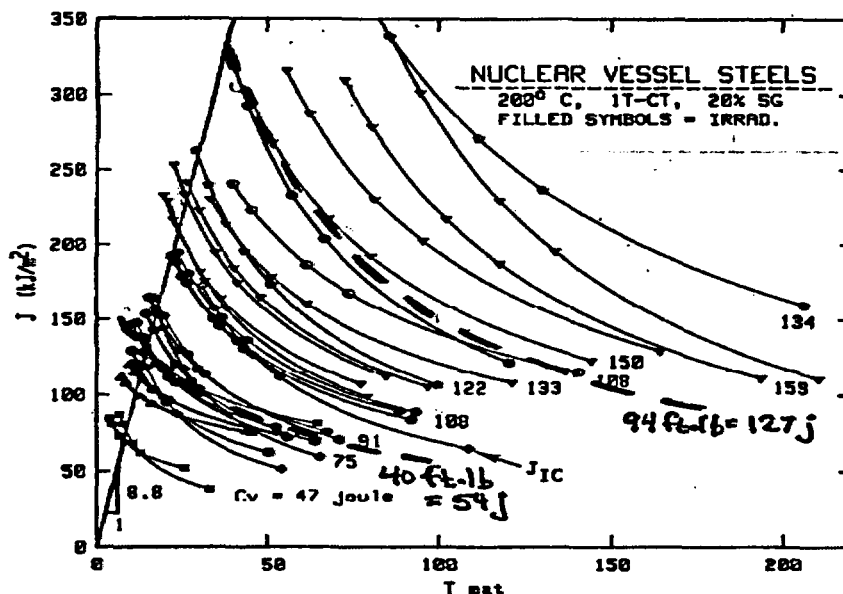


Figure 28: J-T Diagram for several reactor vessel steels and welds showing correlation with Charpy V-notch Upper Shelf Energy [14]. Power law correlations used for ANO-1 Head (40 and 94 ft-lbs) also shown as "dashed lines" with Charpy absorbed energy marked.

- 2) The constant "C" is also obtained using a graph from Reference 14. The Charpy USE of 94 ft-lb and ANO-1 RVH absorbed energy of

Technical Report to Support Relief Request ANO1-R&R-006

40 ft-lb are divided by 100 and represent the value to be used on the X-axis. The value for "C" is obtained as shown in Figure 29.

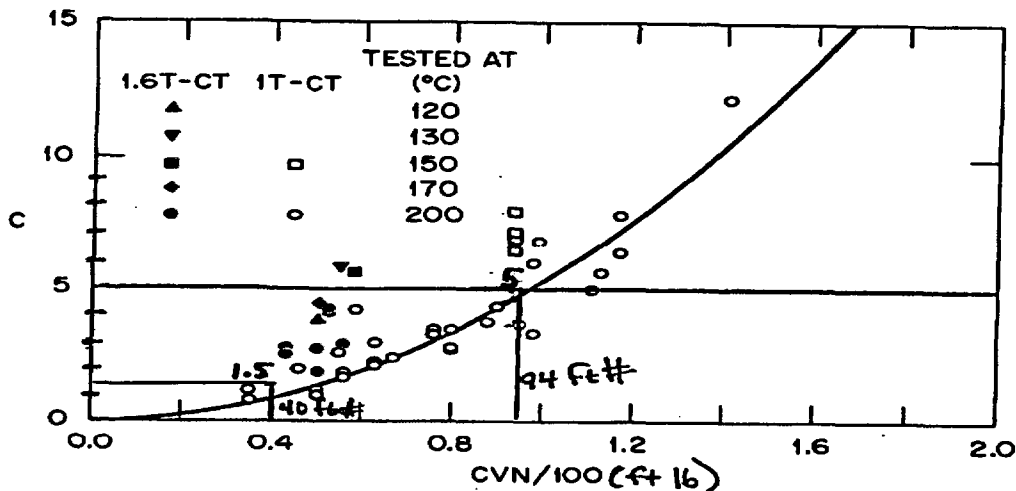


Figure 29: Correlation of coefficient "C" of Power Law J R-curve representation with Charpy V-notch Upper Shelf Energy [14]. Shown is the value for "C" for the two values used in the current analysis.

- 3) The constant "m" is obtained from a graph obtained from Reference 14 and using the values for constant "C". This is shown in Figure 30.

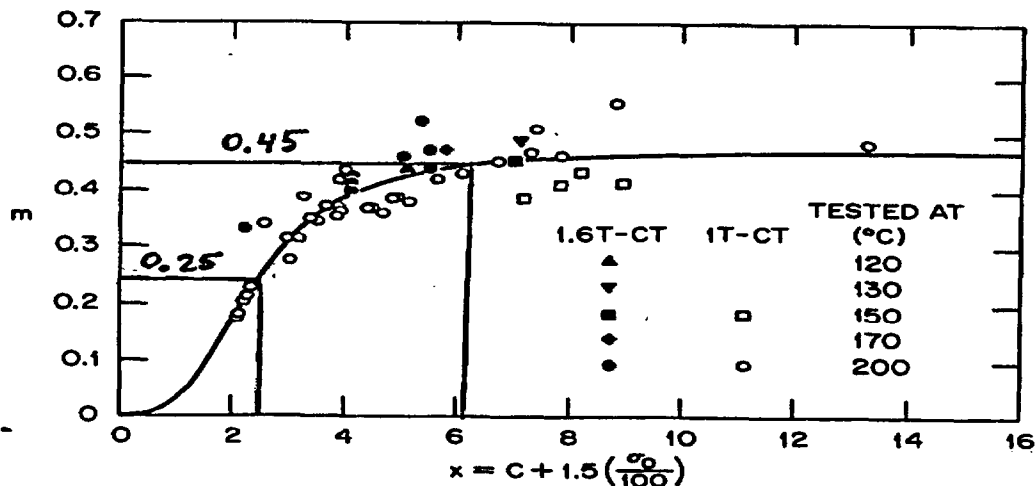


Figure 30: Correlation of constant (exponent) "m" of power law J R-curve representation with coefficient C and flow stress σ_0 [14]. The flow stress is as defined earlier. The values for "m" are shown.

- 4) Once the required constants are obtained the J-R curve for the material specific values were generated in an iterative manner.

Technical Report to Support Relief Request ANO1-R&R-006

Determination of J-integral for Postulated Crack

The determination for the applied "J" was accomplished by using the SIF value from the LEM analysis results presented in Table 1. The values used were for the design minimum chamfer repair as mentioned earlier. The determination of "J" used the guidance from Appendix K of Reference 8. This guidance is based on generic conversion from SIF to "J" and is not geometry specific. Hence this conversion applies to the current work. Additional justification for the use of estimating "J" from the SIF (or "K") can be found in Reference 16. In this reference it is shown that the conversion is valid under "small scale yielding" since the J-integral is equivalent to the "strain energy release rate (G)" under small scale yielding conditions. The small scale yielding conditions apply when the plastic zone size ahead of the crack tip is small compared to the flaw size and the dimensions of the component. As will be shown later, this condition is met for the postulated J-groove weld crack. The conversion obtained from Appendix "K" is as follows:

$$J = \frac{(K'_{Ip} + K'_{Ir})^2}{E'}$$

Where:

J = J-integral ({in-kip}/in²)

K'_{Ip} = The SIF for primary stress, corrected for small scale yielding (ksi√in)

K'_{Ir} = The SIF for residual stress, corrected for small scale yielding (ksi√in)

$E' = E/(1-\nu^2)$; where E is the Young's Modulus and ν is Poisson's ratio (ksi)

The small scale yielding correction for flaw size, which is obtained from Appendix "K" of Reference 8 and corroborated in Reference 16, is a material characteristic and not geometry dependent, and hence is applicable to the current work. The small scale yielding corrected flaw size is represented by:

$$a_e = a + (1/6\pi)[(K_{Ip} + K_{Ir})/\sigma_{ys}]^2$$

and r_p can be defined as $r_p = (1/6\pi)[(K_{Ip} + K_{Ir})/\sigma_{ys}]^2$; thus $a_e = a + r_p$

Where:

a_e = Small scale yielding corrected flaw size (inch)

a = Postulated flaw size (inch)

K_{Ip} = SIF for primary stress {from LEM analysis, Table 1} (ksi)

K_{Ir} = SIF for residual stress {from LEM analysis, Table 1} (ksi)

σ_{ys} = Material yield strength at temperature (ksi); and,

r_p = Plastic Zone Size {PZS} (inch)

Technical Report to Support Relief Request ANO1-R&R-006

The required material properties were obtained from ASME Code Section II, Part D at operating temperature as follows:

$$\begin{aligned} E &= 28.0 \cdot 10^3 \text{ ksi} \\ \nu &= 0.3 \\ E' &= 30.769 \cdot 10^3 \text{ ksi} \\ \sigma_{ys} &= 60.0 \text{ ksi} \end{aligned}$$

Since the SIF (K) is directly proportional to \sqrt{a} , it follows that:

$$K'_{ix} = K_{ix} \cdot \sqrt{\frac{a_e}{a}}$$

Where the subscript index "x" equals "p" for primary stress and equals "r" for residual stress. The other quantities are as defined before.

The tearing modulus (T) is defined as [14 and Appendix K of Reference 8] as:

$$T = \frac{E}{\sigma_{flow}} \cdot \frac{dJ}{da}$$

Where:

$\frac{dJ}{da}$ = The slope of the J versus crack length curve, and the other quantities are as defined earlier.

For the applied "J-T" relationship two crack (flaw) lengths are needed to define the slope ($\frac{dJ}{da}$). This can be accomplished by using the postulated flaw size and the small scale yielding corrected flaw size. Because of the sharp gradient of the stress distribution near the crack front in the present application (shown in Figures 10 and 11), a check analysis to ensure the accuracy of the small scale yielding correction (plastic zone size) was performed. This was accomplished by using the LEFM finite element analysis, described earlier, to evaluate the SIF for a larger flaw. This analysis [17] was performed by increasing the original flaw size of ≈ 1.5 inches by 0.4 inch. The SIF results from this analysis are shown in Figure 31. From the information obtained from Reference 17 a comparison of the SIF obtained by the two methods showed that the small scale yielding correction is valid. This comparison is presented in Table 2.

Technical Report to Support Relief Request ANO1-R&R-006

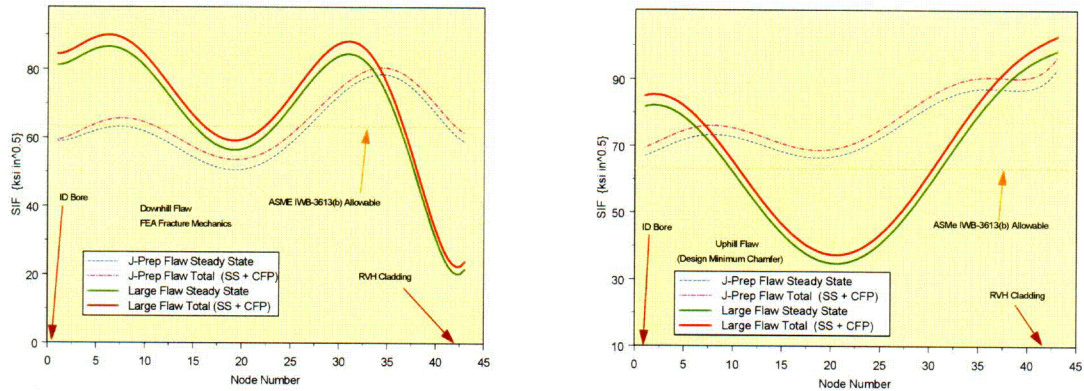


Figure 31: Comparison of SIF for the postulated flaw and larger flaw. The postulated flaw is ≈ 1.5 inches and the larger flaw is ≈ 1.9 inches. The left graph is for the downhill flaw and the right graph for the uphill flaw. In both graphs the solid curves are for the larger flaw size and the dashed curve for the postulated flaw size.

Table 2: Comparison of SIF (Small scale yielding and FEA)

	$\sqrt{(a_0/a)}$	K small scale yielding approximation (ksi \sqrt{in})	K from FEA (ksi \sqrt{in})
Postulated Crack (1.5 inches)		94.4	94.4 ¹
Extended Crack (1.9 inches)	1.125	106.2	103.3 ²

- 1) From Reference 11.
- 2) From reference 17.

The results presented in Table 2 show that the SIF from small scale yielding to be conservative.

The analysis for the postulated crack, using the EPFM methodology presented above, was performed. The results from the analysis are presented in Table 3 and graphically presented in Figure 32. In Table 2 the SIFs and resulting “J” values corresponding to the various safety factors used in the current work are presented. It should be recognized that the high safety factors of 3.5 and 4.0 are presented to show a comparison and they are not used to justify the proposed safety factors. The instability point (4.4 in-kip/in²) is obtained by the intersection of the material curve and the applied stress line in Figure 32, and is also presented in the table in a red font. The result for the proposed safety factor (3.0 on primary stress and 1.5 on residual

Technical Report to Support Relief Request ANO1-R&R-006

stress) is shown in blue font. As can be seen from Table 3 the applied “J” for the proposed safety factor is considerably lower than the “J” at instability (0.853 vs. 4.4). This indicates that sufficient margin against instability exists for the proposed safety factor. This is also observed in the graph presented in Figure 32.

Table 3: J-T Computations for ANO-1 RVH J-groove Weld Remnant Crack using EPFM (guidance from Appendix K of Reference 8) Methodology.

Safety Factor (SF)	K_{ip}	K_{ir}	K_{total}	r_p (Plastic Zone Size)	a_e	$\sqrt{(a_e/a)}$	K'_{total}
	ksi/in			inches			ksi/in
SF=1	3.7	90.7	94.4	0.131	1.631	1.043	98.4
*SF=3, 1.5	11.1	136.1	147.2	0.319	1.819	1.101	162.0
SF=2	7.4	181.4	188.8	0.525	2.025	1.162	219.4
SF=3	11.1	272.1	283.2	1.182	2.682	1.337	378.7
SF=3.5	13.0	317.5	330.4	1.609	3.109	1.440	475.6
SF=4	14.8	362.8	377.6	2.101	3.601	1.549	585.1

Safety Factor (SF)	K_{ip}	K_{ir}	K_{total}	K'_{total}	J'_{total}	T	J @ Instability
	ksi/in				In-kips/in ²		In-kips/in ²
SF=1	3.7	90.7	94.4	98.4	0.315	0.916	4.4
*SF=3, 1.5	11.1	136.1	147.2	162.0	0.853	2.483	4.4
SF=2	7.4	181.4	188.8	219.4	1.564	4.551	4.4
SF=3	11.1	272.1	283.2	378.7	4.660	13.559	4.4
SF=3.5	13.0	317.5	330.4	475.6	7.353	21.392	4.4
SF=4	14.8	362.8	377.6	585.1	11.125	32.367	4.4

- *Appropriate Safety Factor case for ductile material: SF=3 on primary, 1.5 on residual stress.*
- *The light green font represents results for much higher safety factors and shown for informative comparison purposes only.*

The standard J-T instability analysis approach, described in Appendix K of Reference 8, shows that instability is reached when the material J-T curve intersects the applied J-T line. In Figure 32 this occurs at a “J” value of 4.4 in-kip/in². It also seen in Figure 32, that the extremely low value for USE of 40 ft-lb indicates that sufficient margin against instability is assured for the proposed safety factor. The instability point for the extremely low USE is at the intersection of the LEMF material toughness (K_{Ic}) line. In addition the Charpy data presented in Figure 27, showed that the data at +10 °F was in the lower

Technical Report to Support Relief Request ANO1-R&R-006

transition region where the EPFM methodology is not applicable (EPFM methodology is applicable in the upper shelf region). Therefore, the use of a lower bound USE (94 ft-lb) based material toughness curve is appropriate for the current work.

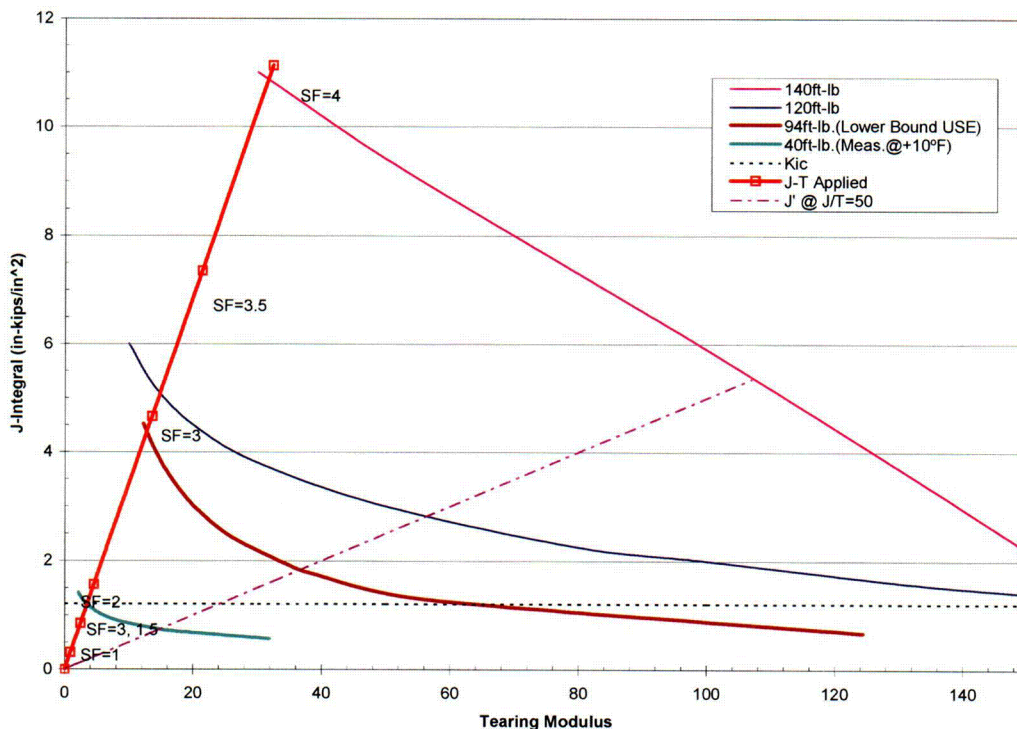


Figure 32: Results of the EPFM stability analysis for ANO-1 RVH J-groove weld remnant crack. The applied line is the solid red colored line. The material toughness curves are shown to the right of this line. The intersection of the applied line and the material curves defines the instability point. The material curve for the current work is the 94 ft-lb curve. Two other USE curves (120 ft-lb and 140 ft-lb) are shown for information purposes. The lowest material curve is for the assumed 40 ft-lb absorbed energy obtained for the ANO-1 RVH materials based on a single temperature test. This value for the absorbed energy is not representative of the actual material's USE, and hence is shown for a very worst case lower bound. The dash-dot line to the right of the applied line represents the slope of the cut-off line in Figure 28 and is represented by $J' @ J/T=50$.

The purpose of showing the $J' @ J/T=50$ line is to show that the Charpy USE and "J" correlation, presented in Figure 28, is truncated at this line. Therefore the material toughness lines between this line and the applied load line (red line in Figure 32) is an extrapolation of the material toughness. Though it may be argued that such an extrapolation is not justified, information presented in References 18 and 19 indicates that for higher upper shelf materials this limitation is not considered applicable. Therefore the use of the lower bound USE of 94 ft-lb and extrapolation to obtain the instability point is considered valid.

C26

Technical Report to Support Relief Request ANO1-R&R-006

Nonetheless, if the truncation were to be made at the $J'@J/T=50$ line the instability point for the 94-ft-lb USE would be approximately 1.8 in-kip/in². This value is greater than the value for the proposed safety factor by more than a factor of two (0.853 versus 1.8). This demonstrates that there is more than sufficient conservatism built into the proposed safety factor for the ANO-1 RVH, when considering the postulated crack as encompassing the entire J-prep.

Evaluation of the Impact of the New Repair Weld on remnant J-groove Weld

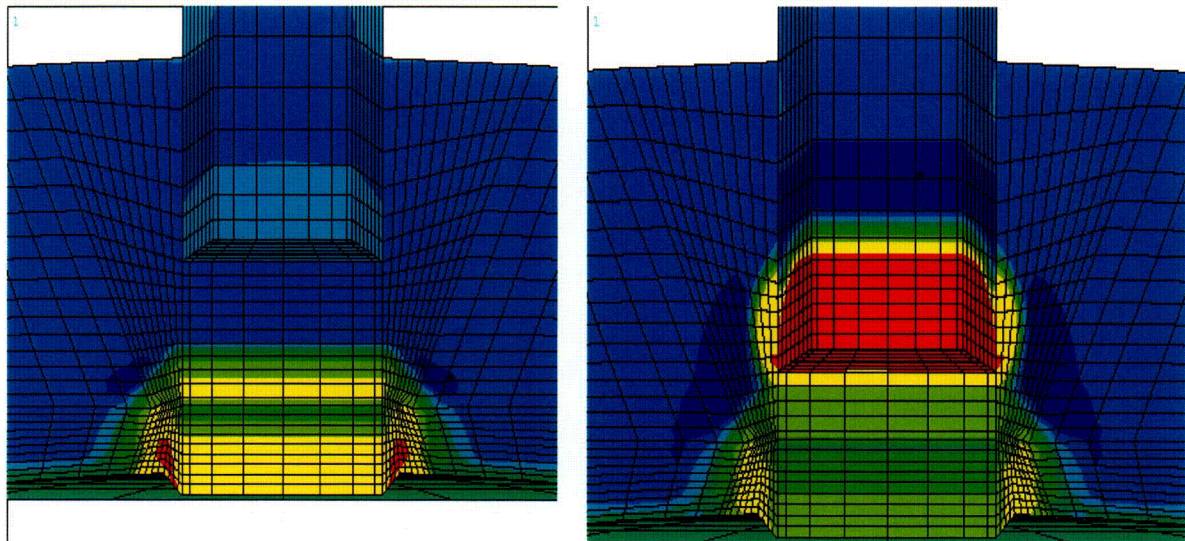
The design repair for the CRDM nozzles at ANO-1 introduces a new weld to attach the CRDM nozzle to the RVH. This weld is located ≈ 2.0 inches above the top of the uphill J-groove weld. The purpose of this section is to present the evaluation of the impact of this new weld on the remnant J-groove weld. This evaluation is performed by comparing the effect on the residual stress distribution at the J-groove weld location before and after the new repair weld is made. Since the SIF for the current work was obtained by using the residual stress distribution at the J-groove weld, using finite element based LEFM method; a comparison of the stress distributions should provide ample and sufficient information to evaluate the effect. This comparison is made by using the stress contours obtained from Reference 20. The stress contours for the hoop stress and axial stresses for the two cases considered are provided in Figures 33 and 34 respectively. In both figures the left picture is the condition for the nozzle counterbored condition and the right picture is for the condition after the new repair weld has been made. The contour colors are the same as defined earlier in the stress analysis section.

The comparison presented in Figure 33, for the hoop stress shows that the stress distribution at the J-groove weld remnant is softened by the installation of the new repair weld. Note that the high stress region (red color) at the J-groove weld corner prior to the installation of the new repair weld has disappeared and become softer (yellow color). This indicates that the installation of the new repair weld reduces the magnitude of the prevailing stress distribution, in the vicinity of the J-groove weld remnant compared to those prior to the installation of the new repair weld. A similar observation is evident from the comparison presented in Figure 34.

Therefore, it is concluded that there is no significant detrimental (increase in stresses) impact on the J-groove weld remnant upon the installation of the new repair weld. On the contrary a beneficial (stress reduction) impact is observed. However, the stress analysis used to provide the stress distribution for the finite element LEFM analysis did not consider the installation of the new repair weld. Hence the stress distribution used in the finite element LEFM analysis is an upper bound stress distribution. This provides added conservatism in the determination of the SIF; that is the estimated SIF is larger than those (SIF) that would be obtained from a simulation which realistically accounted for the full

Technical Report to Support Relief Request ANO1-R&R-006

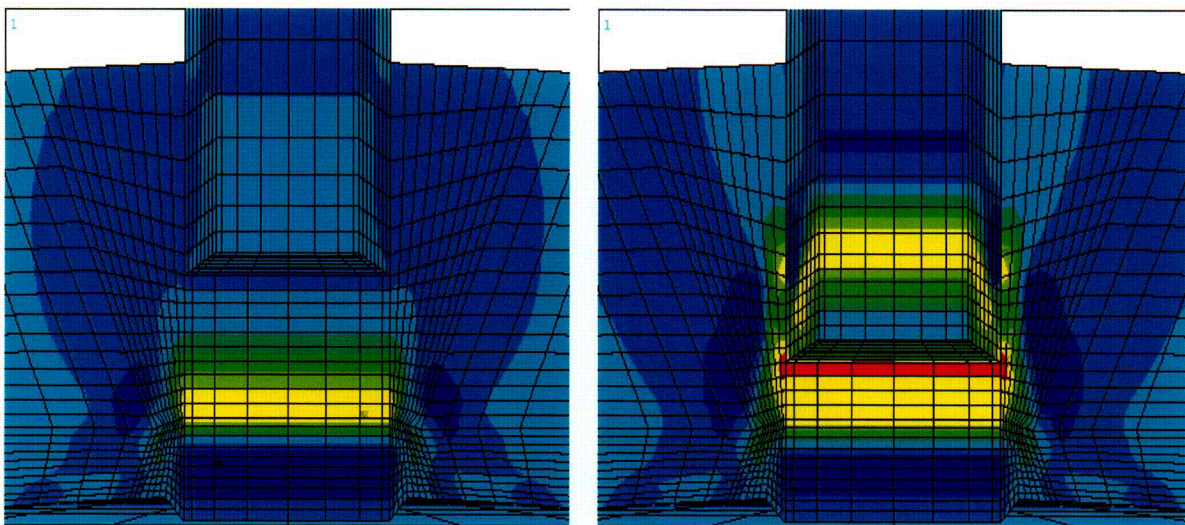
repair process. Thus, the fracture mechanics analysis results are considered to be a conservative upper bound.



Nozzle Counterbored

After New Weld Installation

Figure 33: Comparison of hoop stress distribution before and after installation of new repair weld. Note the high region of stress (red color) in the J-groove weld just after the nozzle has been counterbored (right picture) has disappeared after the installation of the new repair weld (right picture). The red region has changed to yellow indicating a lower magnitude of stress.



Nozzle Counterbored

After New Weld Installation

Figure 34: Comparison of axial stress distribution before and after installation of new repair weld. Similar reduction, albeit to a smaller degree, is observed for the axial stress distribution.

Technical Report to Support Relief Request ANO1-R&R-006

Discussion:

Consideration of Residual Stress

The impact of residual stress on fracture behavior is succinctly presented in Reference 22. In the work presented it was shown, by detailed analysis and experimental testing, that residual stress resulting from welding alters the constraint at the crack tip and simultaneously affects the crack driving force. The analytical effort included detailed finite element analysis and micromechanical modeling. The experimental effort included fracture mechanics testing. The results of the various evaluations showed that the influence of residual stresses was much greater for brittle fracture than for ductile fracture. The importance of adequate representation of the residual stress field to assess fracture conditions was demonstrated.

The work presented in Reference 22 clearly demonstrates the significance of residual stress in the fracture analysis of welded structures. Therefore, it is imperative that residual stress be properly accounted for in the fracture mechanics analysis using LEFM methods. When residual stresses are not considered, by increasing the flaw size such that the residual stress field becomes insignificant, the significant impact of residual stress on fracture (especially brittle fracture) is ignored. Such an analysis will not assess the true potential for brittle fracture and will provide a false margin against brittle fracture. Therefore, a proper and rigorous analysis to evaluate the margin against brittle fracture must adequately consider (and represent) the impact of residual stress.

ASME Code Consideration

The allowable SIF based on IWB-3613(b) [8] is 63.2 ksi $\sqrt{\text{in}}$ for an upper shelf fracture toughness of 200 ksi $\sqrt{\text{in}}$. As shown in the table, the applied SIFs are above the allowed value. The basis for the safety factor of " $\sqrt{10}$ " in IWB-3613(b) can be found in Reference 23:

"The acceptance criteria of IWB-3611 on flaw size were developed with the original purpose of maintaining the design margins of Section III. It is well known that the nominal factor of safety for normal and upset conditions is 3. Consider the general relationship between the stress intensity factor and the stress and flaw size at failure based on linear-elastic fracture mechanics, as noted in the following equation:

$$K_{Ic} = \sigma\sqrt{\pi a}$$

where K_{Ic} = the fracture toughness.

It may therefore be deduced that a factor of safety of 3 on stress at failure is consistent with a factor of safety of 9 on flaw size. Code committees tend to

Technical Report to Support Relief Request ANO1-R&R-006

prefer round numbers, so the value of 9 is rounded up to 10 to provide a safety factor slightly higher than the design safety factor.”

Therefore, the safety factor on the SIF, based on the above equation, results in a value of $\sqrt{10}$. The design safety factor value of 3 was based on the ultimate tensile strength of the ferritic material [24], thereby limiting the allowable general primary membrane stress (P_m) to be less than or equal to one-third of the material ultimate strength.

In addition the design rules for Section III of the ASME Boiler and Pressure Vessel Code are defined for primary bending stress (P_b) and local primary membrane stress (P_L) to be lower than $1.5S_m$, which is approximately equal to the material yield strength. Further, the stress range when considering secondary stresses is increased by an additional factor of two to $3S_m$. This increase for local primary stresses then results in a nominal safety factor of 2 with consideration of bending and local stress effects. The limit on secondary stresses was included to prevent gross distortion of Code components.

The aspect of using different safety factors based on loading type was recognized in Appendix G to ASME Section XI [8]. Although this appendix is for “hypothetical flaw analysis” to ensure safety against non-ductile fracture, its applicability to the evaluation of flaws potentially left in the CRDM J-groove welds is appropriate. The current evaluation assumes that the entire J-groove weld for the design minimum chamfer (including the butter) is cracked, which is analogous to postulating a maximum worst case hypothetical flaw. In particular the guidance provided in paragraph G-2222 (Consideration of Membrane and Bending Stresses) notes that; “Equation (1) of G-2215 requires modification to include the bending stresses which may be important contributors to the calculated K_I value at a point near a flange or nozzle”. Therefore the controlling SIF equation, based on material toughness, was defined as:

$$K_{Ia} \geq 2(K_{Im} + K_{Ib})_{Primary} + (K_{Im} + K_{Ib})_{Secondary}$$

where:

K_{Ia} = the available fracture toughness based on crack arrest for the corresponding crack tip temperature;

K_{Im} = the applied SIF due to membrane stress; and,

K_{Ib} = the applied SIF due to bending stress

In Appendix G, the distinction between primary and secondary stresses are recognized by using a safety factor of 2 on primary stresses and a safety factor of 1 on secondary stresses.

The safety factor considerations in the Code (Section III and Appendix G of Section XI) are based on the through-wall stress distribution, which is also the consideration for IWB-3600 of Section XI [8]. However, the safety factor

Technical Report to Support Relief Request ANO1-R&R-006

presented in IWB-3613(b) considers the same safety factor for all stresses. This results in an overly conservative allowable SIF when the predominant loading mechanism is highly localized and due to residual stresses.

A more reasonable approach would be to utilize the philosophy of Appendix G to Section XI [8] and the safety factors utilized in Section III. This approach would result in the governing equation for SIF as:

$$K_{Ia} \geq 3.0(K_{Im} + K_{Ib})_{Primary} + 1.5 (K_{Im} + K_{Ib})_{Secondary \text{ (or Residual)}}$$

In the above equation the primary stresses would be those from operating pressure, which are the only non-displacement limited load on the top head. The secondary stresses would be those due to local structural discontinuity effects and thermal gradients. The safety factors applied are determined by multiplying those in Appendix G by a factor of 1.5. In this manner the appropriate safety margin against non-ductile fracture would be maintained in a manner similar to that prescribed by Appendix G of Reference 8 but with a higher safety factor. However, as shown in Table 1 and 3 and Figures 10 and 11, the predominant stresses are due to residual stress. Hence, this proposed safety factor will provide an additional conservatism when compared to that in Appendix "G" of Reference 8.

Using the results from the EPFM analysis, Table 3 and Figure 32, it is observed that the proposed safety factor (3.0 on primary stress and 1.5 on the residual stress) provides sufficient margin against instability. In fact the margin is a factor of 5.16 (4.4/0.853) against instability. Inherent in this calculation are conservatisms associated with the stress analysis (no consideration for stress reduction due to the new repair weld) and the lower bound USE used to determine the material toughness. Therefore, the analysis presented herein clearly demonstrates that the proposed safety factor will provide sufficient margin against instability for the postulated crack (entire J-prep assumed cracked).

The same proposed safety factor (3.0 on primary stress and 1.5 on the residual stress) can be used to evaluate the adequacy of margin using the LFM results for the minimum design chamfer case of Table 1, as follows:

$$3.0(K_{Im} + K_{Ib})_{Primary} + 1.5(K_{Im} + K_{Ib})_{Secondary \text{ or Residual}} \leq K_{Ia}$$

$$\begin{aligned} 3(3.7)_{Operating \text{ Condition}} + 1.5(90.7)_{Residual} &= 147.15 \leq 200 \text{ Uphill Flaw} \\ 3(3.01)_{Operating \text{ Condition}} + 1.5(76.99)_{Residual} &= 124.5 \leq 200 \text{ Downhill Flaw} \end{aligned}$$

Thus both the EPFM and LFM methods show that adequate margin exists. The EPFM method demonstrates margin against instability at operating conditions, whereas the LFM method demonstrates margin against non-ductile failure. Since the EPFM method is more appropriate for the operating conditions,

Technical Report to Support Relief Request ANO1-R&R-006

as indicated by the screening criterion, the proposed safety factor is justified on this basis.

The analysis presented in the preceding sections required significant analytical resources to adequately characterize the primary and residual component stresses. It was also demonstrated that the predominant stress contributing to the high SIF was from the residual stress. The residual stress is highly localized and would decay to very low values at some distance beyond the weld butter to low alloy steel interface. Thus, an alternative approach that would simultaneously conserve analytical resource and at the same time provide adequate margin could be considered. However it must be emphasized that this approach would be limited to applications such as this one where the highly localized stress governs the SIF behavior at the crack tip. A safety factor to be applied to the total stresses can be deduced from the structure of the safety factor for primary bending and primary local membrane stresses defined in Section III. It was observed that the safety factor for these stresses was two-thirds of that for the general primary membrane stress. In addition the fracture mechanics analysis for the current evaluation demonstrates that the predominant loading is due to the localized residual stress distribution. Thereby, applying a safety factor of 2 to the total stresses would also be appropriate. Thus the allowable SIF would be as follows:

$$2 * K_{total} \leq K_{Ia} \text{ or } K_{total} \leq K_{Ia} / 2$$

The safety factor of 2 on the total stress from the EPFM results, both in Table 3 and in Figure 32, demonstrates that adequate margin against instability exists. The margin is a factor of 2.81. Using the results from the LEFM analysis, for the design minimum chamfer case in Table 1, leads to the following result:

$$\begin{aligned} 2(94.4) &= 188.8 \leq 200 \text{ Uphill Flaw} \\ 2(76.99) &= 153.98 \leq 200 \text{ Downhill Flaw.} \end{aligned}$$

This simpler form also demonstrates that adequate margin exists. However, as stated earlier this safety factor would only apply for conditions when the highly localized stress significantly contributes (dominates) to the SIF at the crack tip. This safety factor of 2.0 is only provided for information and is not to be construed as a proposed safety factor.

The pertinent results from all of the analyses are summarized in Table 4. In this table the applied parameter is compared to the limiting parameter and from that a ratio, which describes the margin against the appropriate failure criterion, is developed. This margin then succinctly provides a numerical estimate of the structural integrity of the ANO-1 RVH. The comparison also shows that using the proper evaluation method for the ANO-1 RVH, which is the EPFM method, significant margin against failure is demonstrated.

Technical Report to Support Relief Request ANO1-R&R-006

Table 4: Comparison of the Analyses Results

Safety Factor (Applied)	Applied Parameter (AP)		Limiting Parameter (LP)		Margin Against Failure	
	EPFM J (in-kip/in ²)	LEFM K or SIF (ksi√in)	EPFM J (in-kip/in ²)	LEFM K or SIF (ksi√in)	LP/AP	
					EPFM	LEFM
1.0 (As Evaluated Stresses)	0.315	94.4	4.4	200.0	13.97	2.12
3.0, 1.5 3.0 - Primary 1.5 - Residual	0.853	147.5	4.4	200.0	5.16	1.36
2.0 on both; Primary & Residual	1.564	188.8	4.4	200.0	2.81	1.06
3.0 on both; Primary & Residual	4.66	283.2	4.4	200.0	0.94	0.71

The evaluation provided above show that there is a significant margin against either flaw instability (EPFM) or brittle fracture (LEFM) with the use of the proposed safety factor (and acceptance criteria). In addition, the overall approach is conservative in that:

1. The fracture mechanics evaluation has been based on a hypothetical flaw that is assumed to exist in the entire J-groove weld at the highest stress locations.
2. The evaluations based on EPFM methods demonstrate that sufficiently high margin against flaw instability exists. In addition the LEFM method also demonstrates that considerable safety against brittle fracture exists.

Technical Report to Support Relief Request ANO1-R&R-006

Conclusions

The analysis and discussions presented in this report support the following conclusions:

- 1) The stress distribution in the J-groove weld and its immediate vicinity is dominated by the residual stresses created by welding. These stresses are shown to be very localized and confined to the J-groove weld region.
- 2) The stress analysis is conservative because the analysis did not consider the reduction in the stress distribution at the J-groove weld remnant caused by the installation of the new repair weld.
- 3) The importance for considering residual stress has been demonstrated. This conforms to the NRC expectation cited in Reference 13.
- 4) The stress distributions in the J-groove weld region are not amenable to characterization by either a third order polynomial or a linearized stress representation. This precludes the use of known empirical closed form solutions to estimate the SIF at the crack front. The proper method to estimate the SIF along the crack front is by a finite element method. Thus, proper consideration of residual stress and its contribution to the propensity for brittle fracture can be accurately determined by finite element methods.
- 5) The preferred method for determining the SIF is to properly consider all the prevailing loading conditions (residual, operating and internal pressure on crack face), which is the expectation stated in Reference 13, to ensure accurate characterization of the propensity for brittle fracture. Such an effort does result in the SIF exceeding the ASME Section XI IWB-3613(b) allowable.
- 6) Considering the evaluation for safety factors utilized in the ASME Code, a rational justification for an alternate safety factor is proposed. The proposed safety is justified because it considers the distinction between general membrane and the local membrane stresses, and is in accordance with the design rules of Section III of the ASME Code.
- 7) An EPFM evaluation for the design minimum chamfer, using an acceptable methodology and the proposed safety factor, has demonstrated that adequate margin against flaw instability exists.

Technical Report to Support Relief Request ANO1-R&R-006

- 8) The LEFM methodology, using the proposed safety factor, also demonstrated that adequate margin against brittle fracture exists.
- 9) The evaluation provided herein, clearly demonstrates that the proposed safety factor, defined as:

3.0 on primary stresses and 1.5 on residual stresses

provides adequate margin against failure.

- 10) The analyses results presented in the previous sections, along with the conservatisms (with respect to the stress analysis and the lower bound USE for material toughness) used in the analysis, demonstrate that adequate margin against failure exists. Therefore, the analysis clearly demonstrates that the structural and leakage integrity of the ANO-1 RVH, based on the postulated J-groove weld remnant flaw encompassing the entire J-prep, is maintained for the remaining life of this RVH.

Technical Report to Support Relief Request ANO1-R&R-006

References

- 1) "ANO-1 CRDM Nozzle IDTB J-groove Weld Flaw evaluation"; Framatome ANP Calculation Number 32-5021538-00; Framatome ANP; November 11, 2002. (Framatome Proprietary Document)
- 2) "Flaw Evaluation Procedures – Background and Application of ASME Section XI, Appendix A"; EPRI Report NP-719-SR; Electric Power Research Institute, Palo Alto, California; August 1978. (EPRI Licensed Material).
- 3) "Structural Life Assessment Methods"; Alan F. Liu; ASM International; Metals Park, Ohio; 1998.
- 4) "ANO Unit 1 CRDM Stress Analysis"; Calculation Number C-4154-00-1; Dominion Engineering Inc. Reston, Virginia; November 2002.
- 5) "PWSCC of Alloy 600 Materials in PWR Primary System Penetrations"; EPRI TR-103696; Electric Power Research Institute, Palo Alto, CA; July 1994.
- 6) BWR Vessel and Internals Project – Evaluation of crack growth in BWR Stainless Steel RPV Internals (BWRVIP-14); EPRI TR-105873; Electric Power Research Institute, Palo Alto, CA; March 1996.
- 7) "BWR Vessel and Internals Project – Evaluation of crack growth in BWR Nickel Base Austenitic Alloys in RPV Internals (BWRVIP-59)"; EPRI TR-108710; Electric Power Research Institute, Palo Alto, CA; December 1998.
- 8) ASME Boiler and Pressure Vessel Code, Section XI; 1992 Edition.
- 9) "CRDM Nozzle ID Temper Bead Weld Repair ANO Unit 1; FTI Drawing number 5021508-03.
- 10) "Principles of Fracture mechanics"; A. J. Sanford; First Edition; Prentice Hall Limited; 2002.
- 11) "Fracture Mechanics Evaluation of ANO-1 Top head CRDM Penetration with J-Groove Weld chamfer Repairs"; G. Angah Miessi; Calculation Number ANO-25Q-310; Structural Integrity Associates, San Jose, CA; April 2004.
- 12) "EPFM Analysis of Potential Remnant Crack in ANO-1 RPV Top head CRDM Nozzle Repairs (Relief request ANO1-R&R-006)"; P. Riccardella; Calculation Number ANO-25Q-311; Structural Integrity Associates, San Jose, CA; April 2004.
- 13) NRC letter, *Request for Additional Information Concerning WCAP-16180NP, Revision 0, "Operability Assessment for Combustion Engineering Plants with Hypothetical Flaw Indications in Pressurizer heater Sleeves" (TAC No. MC1751)* from Mr. D. Holland, Project Manager, Office of NRR, to Mr. G. Bischoff, Manager, owners Group Program Management Office, Westinghouse Electric Company.

Technical Report to Support Relief Request ANO1-R&R-006

- 14) NUREG-0744, Volume 2, Revision 1; "Resolution of the task A-11 Reactor vessel Materials Toughness safety issue"; Appendices C-K; Division of Safety Technology, Office of Nuclear Reactor regulation, U. S. Nuclear Regulatory Commission, Washington, D. C. 20555; October 1982.
- 15) NUREG-75/087; U. S. Nuclear Regulatory Commission Standard Review Plan-Branch technical Position 5-2 "Fracture Toughness Requirements for Older Plants" appended to Section 5.3.2 "Pressure-temperature limits"; Office of Nuclear Reactor Regulation; Washington, D.C.; November 1975.
- 16) "Advanced Fracture Mechanics"; Melvin F. Kanninen and Carl H. Popelar; Oxford University Press, Oxford, UK; 1985.
- 17) "Fracture Mechanics Evaluation of ANO-1 Top head CRDM Penetration with J-Groove Flaw Size comparison"; G. Angah Miessi; Calculation Number ANO-25Q-312 (preliminary); Structural Integrity Associates, San Jose, CA; May 2004.
- 18) USNRC Report NUREG/CR-1128; "Structural Integrity of Water Reactor Pressure Boundary Components"; F. Loss, Editor; 1979.
- 19) "Verification of Tearing Modulus Methodology for Application to Pressure Vessels with Low Upper Shelf Fracture Toughness"; S. S. Tang, P. C. Riccardella, R. Huet; Presented at ASTM 2nd International Symposium on Elastic-Plastic Fracture Mechanics, October 6-9, 1981, Philadelphia, PA.
- 20) "ANO Unit 1 Nozzle Repair Weld analysis"; Calculation Number C-4154-00-2; Dominion Engineering Inc. Reston, Virginia; November 2002.
- 21) Calculation No: 86-E-0074-161; "ANO-1 CRDM IDTB Weld Anomaly Flaw evaluations"; Framatome ANP calculation, No: 32-5021539-00; Dated November 5, 2002.
- 22) "Effect of Residual Stress on Brittle Fracture Testing"; Michael R. Hill and Tina L. Panontin; *Fatigue and Fracture Mechanics: 29th Volume, ASTM STP 1332*; T. L. Panontin and S. D. Sheppard, Editors; American Society for Testing and Materials; 1998.
- 23) "Section XI Flaw Acceptance Criteria and Evaluation Using Code Procedures"; Arthur F. Deardorff; Chapter 29, Companion Guide to the ASME Boiler and Pressure Vessel Code, Volume 2; K. R. Rao Editor; ASME Press; 2002.
- 24) "Subsection NB – Class 1 Components"; John Hechmer; Chapter 6, Companion Guide to the ASME Boiler and Pressure Vessel Code, Volume 1; K. R. Rao Editor; ASME Press; 2002.